ASSESSMENT OF SUBSURFACE DAMAGE IN ULTRAPRECISION MACHINED CADMIUM SULFIDE BY FLUORESCENCE MICROSCOPY

By

KIM-CHENG TAN

Bachelor of Science

Oklahoma State University

Stillwater, Oklahoma

1986

Submitted to the Faculty of the
Graduate College of the
Oklahoma State University
in partial fulfillment of
the requirements for
the Degree of
MASTER OF SCIENCE
December, 1996

OKLAHOMA STATE UNIVERSITY

ASSESSMENT OF SUBSURFACE DAMAGE IN ULTRAPRECISION MACHINED CADMIUM SULFIDE BY FLUORESCENCE MICROSCOPY

Thesis Approved:

Don A. Lucca

Thesis Adviser

Ronald L. Dougherty

Gary E. Young

Thomas C. Collins

Dean of the Graduate College

ACKNOWLEDGMENTS

I would like to express my gratitude and appreciation to Professor Don A. Lucca for giving me the opportunity to undertake this project. His insight in the subject matter and advice have helped considerably in overcoming the many hurdles. The financial assistance that he has graciously given is deeply appreciated.

I would like to give thanks to the members of my advisory committee, Professor Ronald L. Dougherty and Professor Gary E. Young for taking the time to scrutinize my work. Thanks are also due to Professor Joel J. Martin who has taken time to introduce me to the physics of fluorescence, Gene Cantwell for his technical assistance, and Eagle Picher Research Laboratory for the technical support.

My colleagues, Matt Klopfstein, Pai Chou and Dr. Yin-Ming Wang at the Tribology Laboratory, were always present to render assistance and with that I would like to extend my appreciation.

The financial support of the Oklahoma Center for the Advancement of Science and Technology (OCAST) is gratefully acknowledged.

Finally, I extend thanks to my family for their patience and support during this endeavor, and my Lord and Savior, Jesus Christ who is always present to listen to my problems.

TABLE OF CONTENTS

Chapter Page

1 Introduction 1

1.1 Objective 2

1.2 Basic Physics Governing Fluorescence 3

1.3 Some Aspects of Material-Removal in Brittle Materials 10

2 Literature Review 13

3 Experimental Procedures 17

3.1 Optical and Imaging System 17

3.2 Specimen Preparation 20

3.3 Fluorescence Intensity Measurements 24

4 Results and Discussion 29

5 Conclusion 46

Bibliography 48

OKLAHOMA STATE UNIVERSITY

LIST OF TABLES

Table		Page
4-1	Summary of the mean, standard deviation, and percent change of the fluorescence intensity measured at different illuminated spot locations and the same illuminated spot location at various durations of UV light exposure for the chemo-mechanical polished specimen	43
4-2	Summary of the mean, standard deviation, and percent change of the fluorescence intensity measured at various durations of UV light exposure from $< 0001>$ CdS machined along $(10\bar{1}0)$ at a depth of cut of 0.1 μm	43
4-3	Summary of the mean, standard deviation, and percent change of the fluorescence intensity measured at various durations of UV light exposure from $< 0001>$ CdS machined along $(10\bar{1}0)$ at a depth of cut of 0.5 μm	44
4.4	Summary of the mean, standard deviation, and percent change of the fluorescence intensity measured at various durations of UV light exposure from $< 0001>$ CdS machined along $(10\bar{1}0)$ at a depth of cut of 1.25 μm	44
4.5	Summary of the mean, standard deviation, and percent change of the fluorescence intensity measured at various durations of UV light exposure from $< 0001>$ CdS machined along $(10\bar{1}0)$ at a depth of cut of 10.0 μm	44
4.6	Summary of the mean and standard deviation of the fluorescence intensity from $< 0001>$ CdS machined along $(10\bar{1}0)$ measured at various depths of cut exposed to 3 hours of UV light	45
4-7	Summary of the mean and standard deviation of the fluorescence intensity from $< 0001>$ CdS machined along $(11\bar{2}0)$ measured at various depths of cut exposed to 3 hours of UV light	45

OKLAHOMA STATE UNIVERSITY

4-8 Summary of the mean fluorescence intensity from < 0001> CdS machined along $(10\bar{1}0)$ and $(11\bar{2}0)$ measured at various depths of cut exposed to 3 hours of UV light 45

AHOMA STATE UNIVERSITY

LIST OF FIGURES

Figures | Page

1-1 Schematic of the process of excitation and luminescence in a hypothetical material having the electronic energy scheme as shown (Imbush, 1978) 4

1-2 Typical excitation spectrum (left) and emission spectrum (right) of a fluorescence material (Rost, 1992) 6

1-3 Schematic representation of the emission transitions in a semiconductor (Blasse and Grabmaier, 1994) 8

1-4 Schematic of the physical processes involved in determining photoluminescence output (Hovel, 1992) 9

2-1 Photoluminescence line scans across the center of an ingot annealed GaAs wafer before chemical treatment and at several elapsed times afterward (Hovel, 1992) 16

3-1 Schematic of the optical system used in this study which features the epifluorescence microscope and intensified charge-coupled device 18

3-2 Spectrum transmission curves of Nikon filter block BV-2A that is used in the study (Nikon Corporation, 1993) 19

3-3 Emission spectra of a 100 W mercury lamp commonly used for fluorescence microscopy (Ploem and Tanke, 1987) 20

3-4 Characteristic hexagonal etch pit structure observed on the etched (0001)Cd face using Nomarski optical microscope 21

3-5 Conventional unit cell for CdS crystal in the wurtzite phase. The a, c, and u cell parameters are indicated in the figure, together with the $(10\bar{1}0)$ and $(11\bar{2}0)$ principal planes (Leo et al., 1991) 22

3-6 The (0001)Cd face showing the orientation of the principal planes, machined surface, and etched surface (Lucca, unpublished work) 23

3-7 Schematic of the orientation of the plane of interest parallel to the y-axis of the microscope x-y table 25

3-8 A display of the software histogram tool which gives both the graphical and statistically analyzed information 26

3-9 Typical luminescence profile (schematic) as a function of a spatial coordinate across a dislocation (Bohm and Fischer, 1979) 28

4-1 Mean fluorescence intensity from a chemo-mechanically polished CdS specimen measured at various locations and durations of exposure to UV light 32

4-2 Mean fluorescence intensity from a chemo-mechanically polished CdS specimen (same as specimen of Figure 4-1) measured at same location and various durations of exposure to UV light 33

4-3 Mean fluorescence intensity from <0001> CdS machined along $(10\bar{1}0)$ at a depth of cut of 0.1 µm at various durations of exposure to UV light 34

4-4 Mean fluorescence intensity from <0001> CdS machined along $(10\bar{1}0)$ at a depth of cut of 0.5 µm at various durations of exposure to UV light 35

4-5 Mean fluorescence intensity from <0001> CdS machined along $(10\bar{1}0)$ at a depth of cut of 1.25 µm at various durations of exposure to UV light 36

4-6 Mean fluorescence intensity from <0001> CdS machined along $(10\bar{1}0)$ at a depth of cut of 10.0 µm at various durations of exposure to UV light 37

4-7 Mean fluorescence intensity from <0001> CdS machined along $(10\bar{1}0)$ at various depths of cut measured after 3 hours of exposure to UV light 38

4-8 Mean fluorescence intensity from <0001> CdS machined along $(11\bar{2}0)$ at various depths of cut measured after 3 hours of exposure to UV light 39

OKLAHOMA STATE UNIVERSITY

4-9 Mean fluorescence intensity from <0001> CdS machined along $(10\bar{1}0)$ and $(11\bar{2}0)$ at various depths of cut measured after 3 hours of exposure to UV light 40

4-10 Comparison of depth profiles for <0001> aligned CdS diamond turned along a preferred cleavaged plane, $(10\bar{1}0)$, at various depths of cut (Lucca et al.,1996) 41

4-11 Maximum damage depth for <0001> CdS machined along the $(10\bar{1}0)$ and $(11\bar{2}0)$ planes at various depths of cut (Lucca et al., 1996) 42

OKLAHOMA STATE UNIVERSITY

Chapter 1

Introduction

Often during the fabrication process, when machining to size and following by ultra-fine finishing, surface and subsurface damage is imparted that can be detrimental to the component surface integrity. For semiconductor materials, subsurface integrity is important in determining the performance of the semiconductor devices. According to Puttick et al. (1994) the depth and nature of the subsurface damage in addition to the surface finish will affect the performance of semiconductor components. Puttick et al. (1994) also note that by observing the nature and extent of the subsurface damage, light can be shed on the mechanism of material removal by ultrafine machining. In a recent review on the challenges and potential solutions of the II-VI semiconductor blue-green laser, Luo and Furdyna (1995) note the increasing importance of optoelectronic devices and list their application in optical data storage, laser printing, flat-panel displays, and optical data communication. Vaccaro et al. (1996) have demonstrated the use of CdS interlayers in improving the performance of InP-based optoelectronic devices, and according to Kim et al. (1993) CdS films are also used as a window material in heterojunction solar cell applications.

Characterization is an important aspect in the development of semiconductor devices, and according to Perkowitz et al. (1994) the semiconductor industry uses many characterization methods that focus on electrical, chemical and other approaches.

Perkowitz et al. (1994) note that optical characterization techniques are widely used in that they can measure a broad range of fundamental material parameters, are nondestructive and non-contact in nature, and require minimal sample preparation. The optical techniques include ellipsometry, infrared spectroscopy, optical microscopy, modulation spectroscopy, photoluminescence (PL), and Raman scattering. According to Perkowitz et al. (1994) PL can detect the presence of impurities and crystalline defects in semiconductors, and according to Stine and Knobler (1992) fluorescence microscopy has been employed "to investigate a variety of physical and chemical phenomena such as the existence of pattern-forming instabilities in monolayers". PL scanning at room temperature, a recent procedure, according to Hovel (1992) has been used to assess the uniformity of various properties of semiconductors rather than examine specific defects. He also notes that "PL scanning has been used as a tool for wafer and ingot qualification since the procedure has proven to have a good correlation between PL contrast and electrical properties".

1.1 Objective

In the present work an attempt is made to use measured fluorescent light intensity as a means to quantify the subsurface damage of ultraprecision machined CdS. When the CdS molecules are excited by light such as ultraviolet light, fluorescent light is emitted. Using an intensified charge-coupled device (ICCD) and imaging software, the fluorescent light intensity can be measured. The objective of this study is to gauge the viability of this technique to quantify subsurface damage of ultraprecision machined single crystal materials in terms of emitted fluorescent light intensity at room temperature. It is expected that for a subsurface that is less damaged, the re-emitted light intensity would be higher than for a crystal which has more damage (Böhm and Fischer, 1979; Pribat et al., 1992; Parillaud et al., 1996; Shreter et al., 1996). As a comparison, previous work by Lucca et al. (1995, 1996) which reported

OKLAHOMA STATE UNIVERSITY

on the use of an ion beam channeling technique for assessing damage of diamond turned CdS at several depths of cut, and the subsurface lattice disorder on regions cut parallel to, and 30 degrees off a preferred cleavage plane, will be used to verify the validity of the thesis, and to establish a subsurface damage scale via the fluorescent light intensity. This low cost technique, nondestructive and non-contact in nature, which requires no sample preparation, can potentially be used as a quality control tool in the semiconductor industry.

1.2 Basic Physics Governing Fluorescence

The fundamental physics which governs luminescence has been presented by Imbusch (1978), Ploem and Tanke (1987), Rost (1992), and Blasse and Grabmaier (1994) and a summary is presented below. Luminescence emission according to Imbusch (1978) involves radiative transitions between electronic energy levels of this material, and the emission is characteristic of the material. There are different types of luminescence depending on the cause of excitation and the nature of the electronic transitions involved. If for example, the excitation energy is obtained from the chemical energy of a reaction, the process is called chemiluminescence, whereas cathodoluminescence results from excitation by a beam of energetic electrons. In PL, the required energy is obtained by absorption of photons, such as ultraviolet or blue light. Fluorescence and phosphorescence are recognized within PL and their distinction lies in the manner of the emission. In fluorescence, the phenomenon involves light which is re-emitted almost instantaneously, whereas in phosphorescence the re-emission takes place after a delay, so that phosphorescent objects continue to glow for some time after the excitation source has been removed.

The fundamental process of excitation and emission in a hypothetical material is illustrated in Figure 1-1. Electrons of molecules or atoms normally exist at the lowest energy state known as the ground state with energy $E_{0,}$ and with corresponding

OKLAHOMA STATE UNIVERSITY

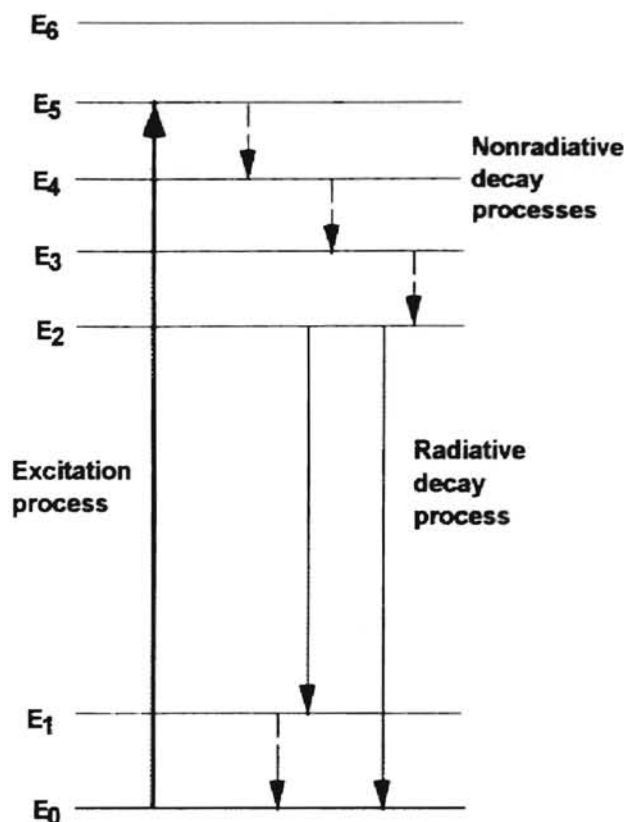

Figure 1-1: Schematic of the process of excitation and luminescence in a hypothetical material having the electronic energy scheme as shown (Imbush, 1978).

rotational and vibrational states. When a molecule is irradiated with light of short wavelength such as ultraviolet light, the electrons acquire energy resulting in an excitation to a higher electronic energy state and a higher vibrational state (referred to as an excited state). In Figure 1-1, E_1 to E_5 represent energies of excited states. The energy gaps among adjacent levels between E_5 to E_2 are small, while the difference between energies E_2 and E_1 is large. Imbusch (1978) notes that if the gap between an excited level and the adjacent lower level is small, the material in that excited state tends to decay non-radiatively via loss of vibration energy and releases the energy as heat to the material. In addition, radiative decay only occurs when the transition is from the higher excited state to an adjacent lower excited state or the ground state

STATE UNIVERSITY

which involves energy difference above a critical value. This results in emission of a photon which gives rise to the phenomenon of luminescence. Consequently with the absorption of energy, the electron in the hypothetical material is raised to the E_5 level, it then loses energy as heat by cascading from level 5 to level 4 and so forth, ultimately ending up on level 2. The gap between levels 2 and 1 is above the critical value, so the material decays radiatively from level 2 emitting a photon, and ending on level 1 or 0. If the material decays radiatively to state 1, it then decays non-radiatively through the small gap to the ground state. So for this hypothetical material, two possible luminescence transitions can occur with frequencies given by ν_0 and ν_1 and with angular velocities given by ω_0 and ω_1, where

$$h\nu_1 = \hbar\omega_1 = E_2 - E_1 \tag{1.1}$$

$$h\nu_0 = \hbar\omega_0 = E_2 - E_0 \tag{1.2}$$

and h is Planck's constant and $\hbar = h/(2\pi)$. Imbusch (1978) notes that it is important to not only know the position and nature of the energy levels involved in the radiative process, but also the position and nature of the other levels which may be involved in the excitation process, and in the non-radiative process whereby the excitation arrives at the radiative level.

According to Rost (1992) the fluorescence normally observed is called Stokes fluorescence named after Sir George Stokes who, in 1852, first observed the mechanism of the absorption-emission process. This fluorescence is re-emission of less energetic photons, having a longer wavelength than the excitation light. Rost (1992) notes that emission at shorter wavelengths than that of excitation may also occur, and this is known as anti-Stokes fluorescence. The additional energy accordingly may come from thermal energy or be associated with a molecule with many highly populated vibrational energy levels. The characteristic spectra of fluorescence are the excita-

OKLAHOMA STATE UNIVERSITY

tion spectrum and the emission spectrum as shown in Figure 1-2. The excitation

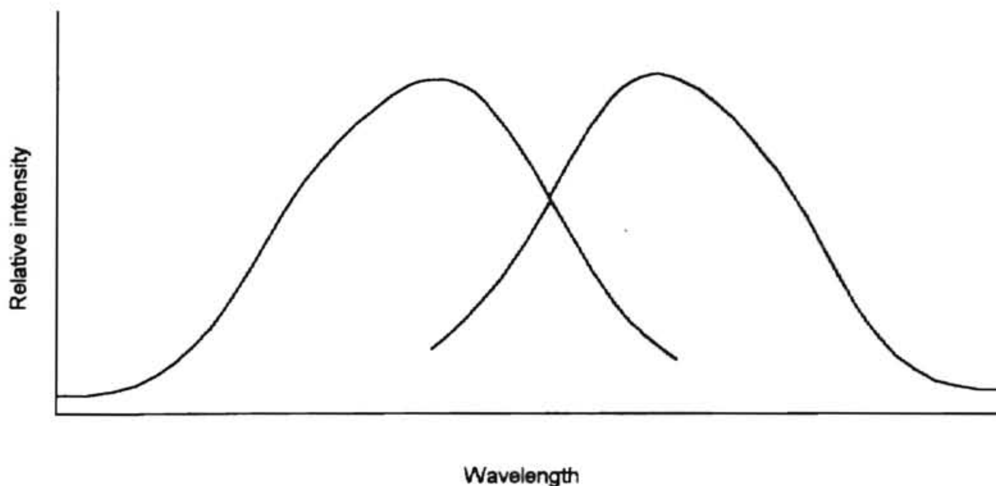

Figure 1-2: Typical excitation spectrum (left) and emission spectrum (right) of a fluorescent material (Rost, 1992).

spectrum (shown as the left-hand curve) is a plot of the relative total intensity of fluorescence obtained when the fluorescent specimen is irradiated at varying wavelengths compared to a given wavelength. An excitation spectral curve according to Rost (1992) has a peak at the photon energy, or wavelength, corresponding to the energy difference between the ground state of the fluorescent material and some favored vibrational level of its first excited state. Ploem and Tanke (1987) note that to obtain intense fluorescence, irradiation with light of wavelengths close to the peak of the excitation spectrum is desirable. The right-hand curve, which is the emission spectrum, is a plot of the fluorescence intensity distribution which results from excitation at a certain wavelength. The shape of the emission spectrum is usually similar to that of the first absorption band, but in 'mirror-image' form.

Semiconductors are characterized by a valence band and a conduction band separated by an energy gap E_g. When subjected to excitation, electrons migrate to the empty conduction band leaving holes in the valence band which was completely filled. According to Blasse and Grabmaier (1994) emission then occurs by electron-hole re-

OKLAHOMA STATE UNIVERSITY

combination usually close to or at defects in the crystal lattice. There are several possibilities for radiative recombination:

1. Edge emission - emission occurs close to the band-gap energy, E_g. This emission is due to exciton recombination of bound excitons where an exciton has either the electron or the hole is trapped at an imperfection in the lattice. Luminescence in CdS is of the exciton emission type (Blasse and Grabmaier, 1994).

2. Deep-center emission - emission occurs at energy considerably lower than E_g.

3. Donor-acceptor pair emission - emission occurs when an electron trapped at a donor and a hole trapped at an acceptor recombine.

4. Other radiative recombination possibilities - for example, a free hole that recombines with a trapped electron or a free electron that recombines with a trapped hole. In these instances the trapped charge carriers may occupy deep traps, so that the emitted energy is considerably less than E_g.

Blasse and Grabmaier (1994) have given a schematic representation of some of the possibilities for radiative recombination in a semiconductor as shown in Figure 1-3. Excitation in excess of the band gap creates electrons in the conduction band and holes in the valence band as depicted in Figure 1-3 by process 1. Optical recombination is shown in processes 2-6. In process 2, a free hole recombines with an electron trapped in a shallow trap level. This is also known as exciton recombination and gives rise to edge emission. Process 3 is the same as 2 only with a deep electron-trapping level. In process 4, a free electron recombines with a trapped hole. Process 5 is donor-acceptor pair emission, and process 6 is electron-hole recombination in an associate of a donor and acceptor.

The processes involved in determining the PL efficiency according to Bebb and Williams (1972) and Hovel (1992) can be distinguished by the following:

1. creation of electron-hole pairs

2. radiation recombination of electron-hole pairs

OKLAHOMA STATE UNIVERSITY

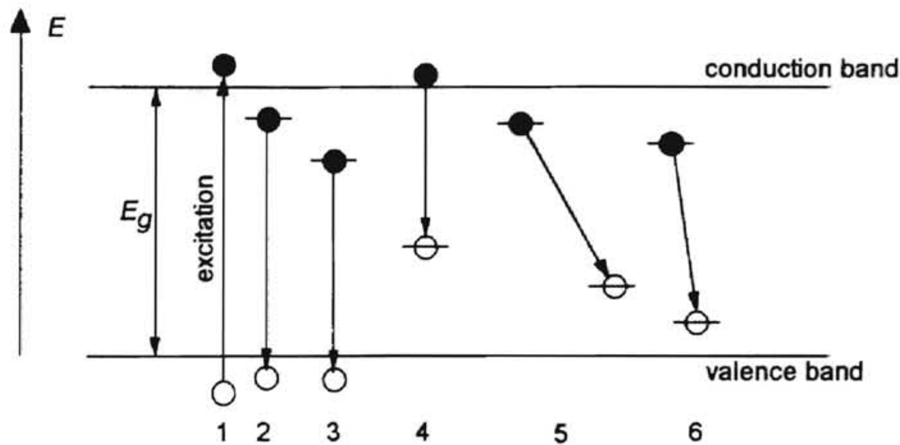

Figure 1-3: Schematic representation of the emission transitions in a semiconductor (Blasse and Grabmaier, 1994).

3. escape of the recombination radiation from the material

4. diffusion into the material

The physical processes involved in determining PL output are shown in Figure 1-4. Hovel (1992) has defined PL efficiency as "the number of photons emitted from the surface versus the number of photons incident". The PL efficiency is therefore determined by competition between the various processes. Hovel (1992) notes that "the low-energy photons created by the radiative recombination may be reabsorbed by the material or emitted from the surface, provided the photon is directed at the surface within the critical angle cone". In addition, "PL photons directed at the back surface have some probability of being reflected back to the front and being included in the emission". Bebb and Williams (1972) note that since the exciting light is absorbed in creating electron-hole pairs, the greatest excitation of the sample is near the surface giving rise to the carrier distribution being both inhomogeneous and nonequilibrium. Thereby in attempting to regain homogeneity and equilibrium, the excess carriers will diffuse away from the surface while being depleted by both radia-

OKLAHOMA STATE UNIVERSITY

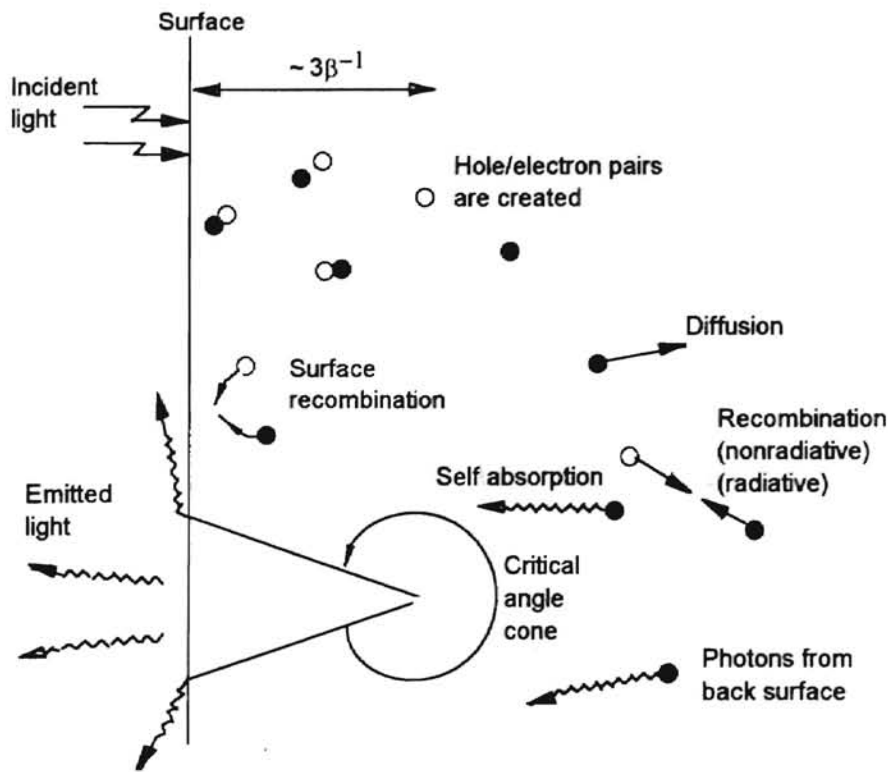

Figure 1-4: Schematic of the physical processes involved in determining photoluminescene output (Hovel, 1992).

tive and nonradiative recombination processes. Accordingly, most of the excitation of the crystal is thereby restricted to a region within a diffusion length (or absorption length) of the illuminated surface. Since the recombination radiation is subjected to self-absorption, it will not propagate far from this region, and the recombination radiation most readily escapes through the nearby illuminated surface. According to Hovel (1992) the incoming light is absorbed in a distance of about $3\beta \leq 1$ μm (where β is the absorption coefficient for that radiation) from the surface. Hovel (1992) has proposed an equation for the PL intensity, F, as a function of the emitted angle Θ accounting for the above-mentioned processes, given by

$$F(\Theta) = \frac{G(1-r)\cos\Theta}{\pi N(N+1)^2}\frac{L}{\tau_R}\frac{1}{S_f} \tag{1.3}$$

OKLAHOMA STATE UNIVERSITY

where G is the incident intensity, r is the reflectivity from the surface, N is the refractive index, L is the diffusion length, τ_R is radiative lifetime, and S_f is the surface recombination velocity. Hovel (1992) notes that comparison with experimental results indicates that the surface recombination velocity determines the overall level of intensity but that the surface non-uniformities (PL contrast) are mainly controlled by L/τ_R and therefore by the ratio of total to radiative lifetime τ/τ_R (since $L = \sqrt{D\tau}$, where D is the diffusion coefficient).

1.3 Some Aspects of Material-Removal in Brittle Materials

One of the goals of an ultraprecision material-removal process is to impart the least amount of surface and subsurface damage possible to the workpiece. This section discusses some recently reported studies on the potential material removal mechanisms in single-point diamond turning (SPDT) of brittle materials.

Blackley and Scattergood (1990) have observed pitting damage which is cutting direction dependent on single point diamond turned germanium single crystal wafers. The pitting damage in turn dictates a limiting feed rate at which the material can be machined. The orientation dependence is attributed to the maximum amplitude of the resolved tensile stresses on {111} cleavage planes. Thus, the pitting damage changes with cutting direction because of the change in crystal orientation with respect to the principal stress axes. Their observations support the assumption that tensile stresses behind the tool tip are responsible for the observed fracture damage.

Morris et al. (1995) in their study of the so-called "ductile regime" SPDT of germanium employed transmission electron microscopy (TEM) and parallel electron energy-loss spectroscopy (PEELS), and contend that material removal takes place in a ductile manner. They support this claim by their examination of the macroscopic morphology of the machining chips, finding that they are smooth and wavy, and do not

exhibit faceting normally indicative of brittle material removal. The machined surfaces that result are smooth and frequently free of cracking. They found no evidence of homogeneous melting, and conclude that the absence of solidified drops or drawn fibers on the machined surface, or in the machining swarf, is conclusive evidence as to the plastic deformation of the material. Morris et al. (1995) rule out conventional plastic deformation modes as there is no dislocation activity evident in the chips. They claim the key to the understanding of the mechanism of plasticity lies in the microstructure of the chip which is in the amorphous phase. This amorphous phase is likely due to a pressure-induced phase transformation. Central to their argument is that the cutting mode, i.e., "ductile regime" machining versus brittle machining is dependent on the depth of penetration or cut. Using the Griffith criteria for brittle fracture as a first approximation, they contend that if the depth of cut taken is of the flaw size, fracture occurs at some critical depth. They then postulate that with a sharp tool resulting in high enough stresses, phase transformation may take place. The region below the tool has high ductility and so "ductile regime" machining is achieved. Phase transformation takes place before cracking, allowing larger depths of cut to be taken before the ductile-to-brittle transition occurs.

In single crystals, there are certain planes that have lower cleavage stresses than others, and therefore machining near the fracture threshold can result in some region which will have a ductile response, and some with a brittle response.

Puttick et al. (1995) in their work on SPDT of silicon present an argument based on the energy scaling of the machining process that leads to a critical depth of cut below which no cracks should accompany the removal of material. The researchers note that from TEM analysis for a surface produced with a depth of cut of 0.5 μm, it is clear that SPDT of silicon has achieved fully ductile removal of material by plastic flow alone. A cross-section of the nano-turned silicon reveals surface deformation consisting of groups of dislocations spaced 50-100 nm apart, which are bundles of elongated loops intersecting the surface, all on the same slip system with a single

OKLAHOMA STATE UNIVERSITY

Burgers vector. This study confirms earlier work on SPDT of silicon by Puttick et al. (1994) which indicated that the main mechanism of material removal was extrusion of plastic material ahead of the tool, which has been observed in low-load indentation by other researchers (Puttick and Hosseini, 1980; Morris and Callahan, 1994). Through TEM observations of turned-surface cross-sections, Puttick et al. (1994) have noted the regularity and homogeneity of the lattice deformation, consisting of elongated dislocation loops lying on a single $(1\bar{1}1)$ plane, and explained that this array has been formed by slip in one or the other of the three $\langle 110 \rangle$ directions lying in the plane. Another observation made was that dislocations were found to lie predominantly in the $(\bar{1}11)$ plane, another possible slip plane, of which the surface trace is parallel to the direction of motion of the tool, that is, in the $[\bar{1}\bar{1}0]$ directions.

OKLAHOMA STATE UNIVERSITY

Chapter 2

Literature Review

Scott and Reed (1975) note that it has been established that in single crystal CdS when free electrons and holes are created in the surface region their subsequent recombination is very dependent upon the condition of the surface and the underlying layer. Therefore, PL due to strongly absorbed primary irradiation will be correspondingly dependent upon the surface. Experimental evidence of this has been provided in the 1950's, 1960's, and early 1970's (Liebson, 1954, 1955; Liebson and West, 1955; Many and Katzir, 1967; Bujatti, 1969; Henry et al., 1970; Ermolovich, 1971). In the late 1970's spatially resolved PL measurements have been used in the investigation of the influence of dislocations on the radiative recombination of electron-hole pairs in III-V compounds materials (Böhm and Fischer, 1978). Recently, PL has been used as a tool in evaluating dislocation density as an indication of crystal quality in the heteroexpitaxy of III-V compounds on silicon substrates (Pribat et al., 1992; Parillaud et al., 1996) and in an experimental investigation of n-ZnSe after plastic deformation (Shreter et al., 1996).

Bleil and Albers (1964) have demonstrated that oxygen is chemisorbed and water vapor physically adsorbed on the CdS surface, causing a decrease and increase in the exciton emission intensity, respectively. The influence of chemisorption of oxygen on the green exciton luminescence and red luminescence observable at room temperature

in CdS single crystals has been investigated by Heine and Wandel (1973). They have observed a reduction of emission in both bands with increase in oxygen pressure. It is clear from all these measurements that chemisorbed oxygen increases the rate of non-radiative recombination, reducing simultaneously the excess free carrier concentration and the radiative recombination rate.

According to Mar (1992) the mechanism of exciton localization at defects of II-VI semiconductors has been discussed in detail by Hopfield (1964) and Halsted (1967). Halsted (1967) has given a comprehensive review of the recombination processes in the near-band-edge region, and has noted that the bound states play a significant role in the near-band-edge transitions. His findings have been confirmed experimentally by Dean et al. (1981) using a different approach. In addition, Mar (1992) notes that PL studies by Henry et al.(1970) of shallow acceptors in CdS, CdSe, Li and Na have established PL as a tool for studying impurity- and defect-related acceptors in II-VI and III-V semiconductors.

Suzuki and Ogawa (1977), Guidotti et al.(1987), and Guidotti and Hovel (1988) have observed that near-band-edge PL emission from GaAs degrades as a function of exposure time to moderate illumination. Guidotti and Hovel (1988) observed the following about this degradation:

1. the degradation rate is independent of incident wavelength, is not governed by a fixed relationship with time, and increases with increasing incident intensity
2. PL degradation is not caused by surface oxidation, and is observed to be faster in an inert atmosphere
3. no degradation is observed at a passivated surface
4. the degradation rate is independent of temperature between 77 and 300 K and at temperatures less than 10 K no PL degradation is observed
5. the effects of degradation do not reverse after a high-temperature annealing

OKLAHOMA STATE UNIVERSITY

cycle

6. the degraded area extends much beyond the illuminated spot, and the observations suggest that PL is brought about by a recombination-enhanced defect reaction (REDR) mechanism near the surface

Hovel (1992) notes that the main process that affects the intensity (but not the distribution) of PL at room temperature is surface recombination, and therefore anything that significantly affects surface states should also affect PL intensity. He has shown that subjecting GaAs wafers to chemical treatment particularly, HCL or NH_4OH significantly enhances the PL intensity. Accordingly the PL initially increases by a factor of three immediately after the treatment, drops back to 2.5 times after 60 minutes and 2 times after 3 hours, and finally saturates permanently at about 1.9 times the original value. He postulates that the chemical treatment removes the native oxide and leaves the GaAs initially in a non-oxidized state after removal with the chemical. Subsequently the native oxide appears to grow back slowly because the surface is temporarily protected by adsorbed Cl, OH, or H ions. The effect of chemical treatment on the PL of an ingot annealed GaAs wafer is shown in Figure 2-1 in which the PL line scans show the effect before immersion in NH_4OH and at various times after.

Negrii (1992) notes that plastic deformation of CdS crystals leads to the appearance of a characteristic group of emission lines in the 505 nm and 515 nm region of the low temperature PL spectrum. He labels this "dislocation emission".

Garosshen et al. (1990) have found that type II-VI semiconductors exhibit significant changes in flow stress when irradiated with light. CdS in particular shows a large photoplastic effect during basal slip which is associated with a large charge on the mobile dislocations. In comparison, prismatic slip exhibits a significantly smaller photoplastic effect and, correspondingly, a smaller charge on the mobile dislocations. This is due to compensating charges along dislocation lines. The photoplastic effect is greatest at light frequencies just below the band gap energy and increases with

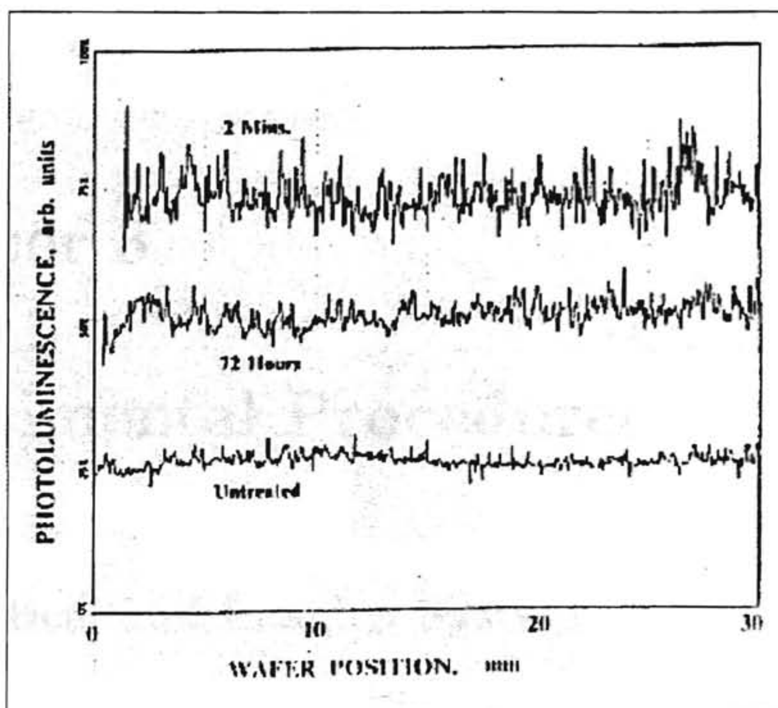

Figure 2-1: Photoluminescence line scans across the center of an ingot annealed GaAs wafer before chemical treatment and at several elapsed times afterward (Hovel, 1992).

light intensity until a saturation level is reached. The magnitude of the photoplastic effect decreases with increasing temperature, and increases with strain rate. They suggest that it may be possible to exploit the photoplastic effect to control dislocation densities in semiconductors which exhibit photoplastic behavior.

OKLAHOMA STATE UNIVERSITY

Chapter 3

Experimental Procedures

3.1 Optical and Imaging System

According to Rost (1992) major sources of instrument error in fluorescence microscopy include instability of the light source, non-homogenous illumination of the object (i.e., illumination with light of uneven intensity or wavelength distribution), and non-linearity of the photometric system. Rost (1992) also notes that optical arrangement is very critical in fluorescence microscopy. The direction of illumination in relation to the direction of measurement affects the relationship between the fluorescent material and the measured fluorescence intensity. The epi-illumination optical arrangement is preferred in fluorescence microscopy. In this optical arrangement, light can be directed downwards onto the specimen from the same side as the objective, or through the objective itself. This technique enables the illumination to be concentrated on, and confined to, the field of view. Light is neither wasted, nor unnecessarily directed at other parts of the specimen, thus minimizing the color-fading area of the specimen. Epi-illumination therefore gives reproducible and ideal conditions which are necessary for quantification purposes.

The optical and imaging system which was used in this study consisted of a Nikon epi-illumination fluorescence microscope with a high intensity 100 W mercury lamp,

a Hamamatsu C3500S intensified charge-coupled device (ICCD), a personal computer with a frame grabber DT3851A from Data Translation, and "GLOBAL LAB Image" imaging software also from Data Translation. The schematic of the optical system which was used is shown in Figure 3-1. The system was mounted on a vibration isolation table.

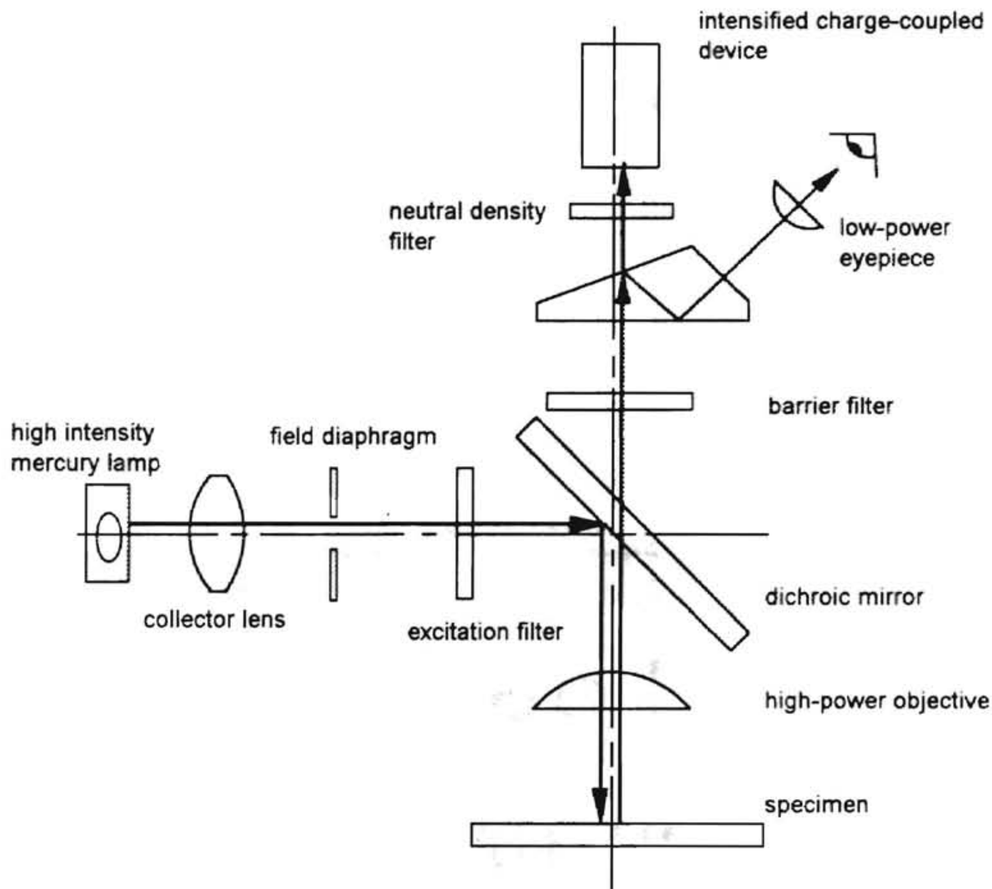

Figure 3-1: Schematic of the optical system used in this study which features the epi-illumination fluorescence microscope and intensified charge-coupled device.

In Figure 3-1, light from the high intensity mercury lamp is concentrated into a beam via the collector lens and directed onto the blue violet excitation filter which permits only light of wavelength between 400 and 440 nm to pass through to the semi-transparent dichroic mirror situated in the body tube of the microscope. The dichroic

mirror or beamsplitter is characterized by a wavelength of 455 nm, above which it preferentially transmits and below which it preferentially reflects. The excitation light of wavelength between 400-440 nm is then reflected by the mirror down through the objective which also acts as a condenser that focuses the excitation light onto the specimen. The fluorescence, excited by the incident beam, is collected by the objective then passes through the dichroic mirror and onto the barrier filter. The barrier filter then permits fluorescence of wavelength of greater than 470 nm to pass through to the eyepiece or ICCD camera. In this study the excitation filter, dichroic mirror, and barrier filter are housed in the Nikon BV-2A filter block. The spectrum transmission curves of the filter block are shown in Figure 3-2. The emission spectra

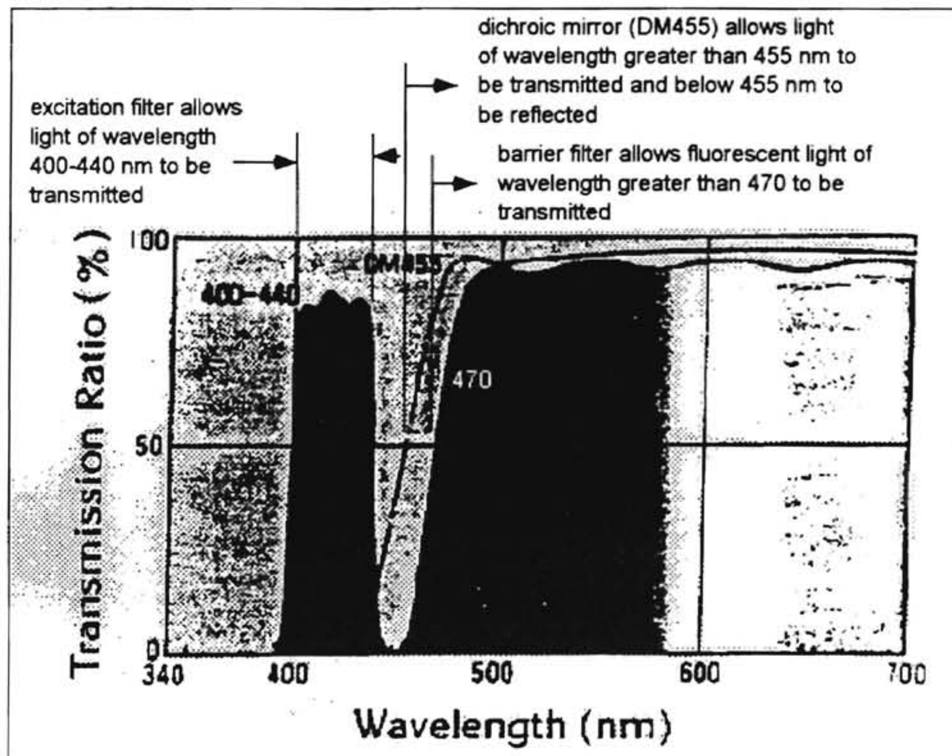

Figure 3-2: Spectrum transmission curves of Nikon filter block BV-2A that is used in the study (Nikon Corporation, 1993).

of a typical 100 W mercury lamp commonly used for fluorescence microscopy is shown

in Figure 3-3 with emission peaks in the region from 300-600 nm.

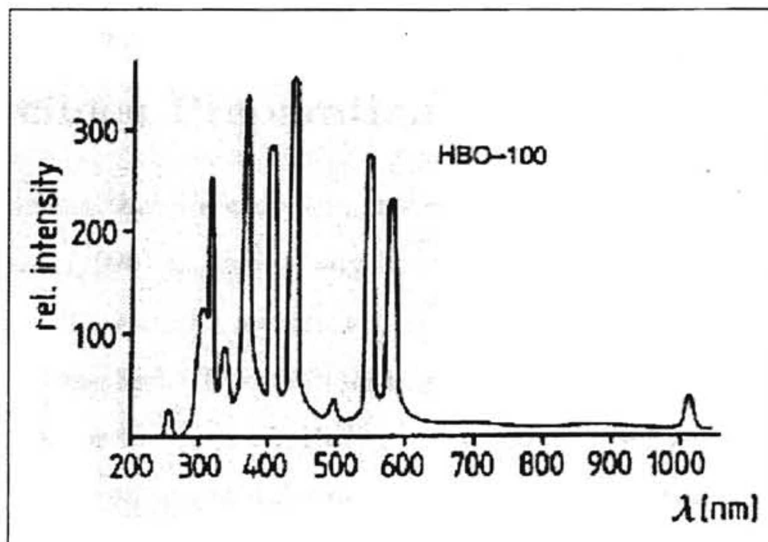

Figure 3-3: Emission spectra of a 100 W mercury lamp commonly used for fluorescence microscopy (Ploem and Tanke, 1987).

The ICCD camera incorporates both the charge-coupled device camera and an image intensifier. The ICCD can measure very low light levels. It is connected in parallel to a monitor (not shown in the schematic), printer, and personal computer with a DT3851A frame grabber board with 256 (8 bit) gray levels. The DT3851A frame grabber is fully software configurable and features high resolution input and display. The intensity of the fluorescence is read via "Global Lab Image" imaging software with display resolution of 640 × 480 pixels. The intensity measurements enabled by the software include point intensity and area histogram (graph, raw data, mean, minimum/maximum, standard deviation, and percent of pixels within target intensity range). The software can display a profile of intensity along a line or an average across several contiguous lines.

Due to the sensitivity of the ICCD, neutral density filters were used to limit the transmission of the fluorescence light so that intensity readings within the grayscale can be obtained. An optimum transmission of 0.1 percent of the re-emitted fluores-

OKLAHOMA STATE UNIVERSITY

cence light was found to give discernible intensity readings with the various specimens. This optimum transmission is used in all the intensity measurements.

3.2 Specimen Preparation

The CdS specimens that were used in this study are the identical specimens used by Lucca et al. (1996) in their study of subsurface damage of CdS assessed by ion channeling. The wurtzite structure CdS used was grown by the physical vapor transport (PTV) method. The (0001)-oriented CdS wafers were sawn from a bulk crystal and etched for 10 minutes in HCl to remove all prior subsurface damage (Lucca et al., 1996). Under an optical microscope the etched (0001)Cd face is observed to have the characteristic hexagonal etch pit structure as shown in Figure 3-4, whereas the (0001)S face does not exhibit such structure.

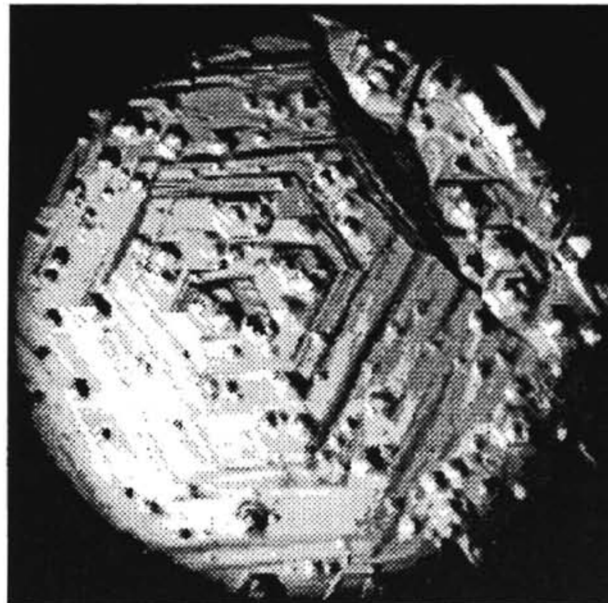

Figure 3-4: Characteristic hexagonal etch pit structure observed on the etched (0001)Cd face observed with a Nomarski optical microscope.

The planes of interest are the principal planes $(10\bar{1}0)$ and $(11\bar{2}0)$ which are parallel to the c-axis, and located 30 degrees apart. The $(10\bar{1}0)$ plane is a preferred cleavage plane and according to Wolff and Broder (1959) the $(11\bar{2}0)$ plane is another cleavage plane. The orientation of the $(10\bar{1}0)$ plane was determined to within about $\pm$ 1 degree by illuminating the (0001)Cd face with a 670 nm light source, and observing the reflected 6-fold star pattern from the etch pits (Lucca et al., 1995). The unit cell for CdS in the wurtzite phase is shown in Figure 3-5.

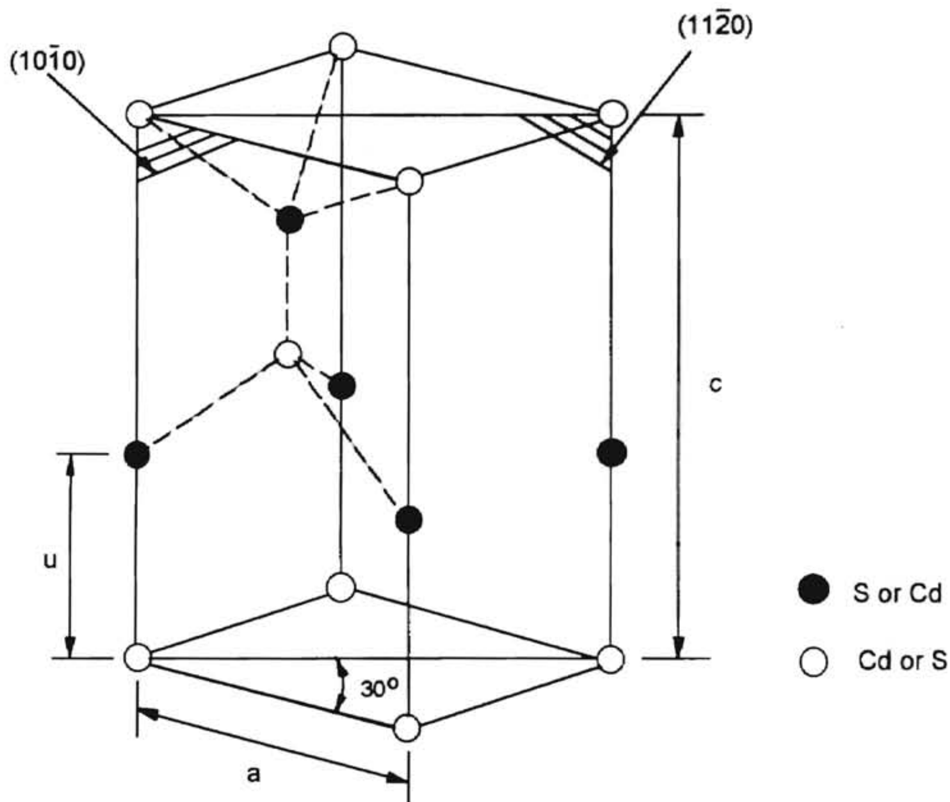

Figure 3-5: Unit cell for CdS in the wurtzite phase. The a, c, and u cell parameters are indicated together with the $(10\bar{1}0)$ and $(11\bar{2}0)$ principal planes (Leo et al., 1991).

The procedure used for SPDT of the CdS specimens has been reported by Lucca et al. (1995) and is repeated here for convenience. The oriented crystals were of nominal dimensions 20 mm $\times$ 25 mm $\times$ 1 mm, and were mounted with instant

OKLAHOMA STATE UNIVERSITY

adhesive to a lapped aluminum substrate which was in turn held on a vacuum chuck of a commercial diamond turning machine. The specimens were positioned with their centerlines approximately 20 mm off the spindle axis, and as a result the cutting direction varied over 60 degrees with respect to the crystallographic direction over the specimen. In this way, machining along both the $(10\bar{1}0)$ and $(11\bar{2}0)$ planes on the same crystal could be achieved. The orientation of the planes and the machined surface is shown in Figure 3-6. A portion of the etched surface was left unmachined

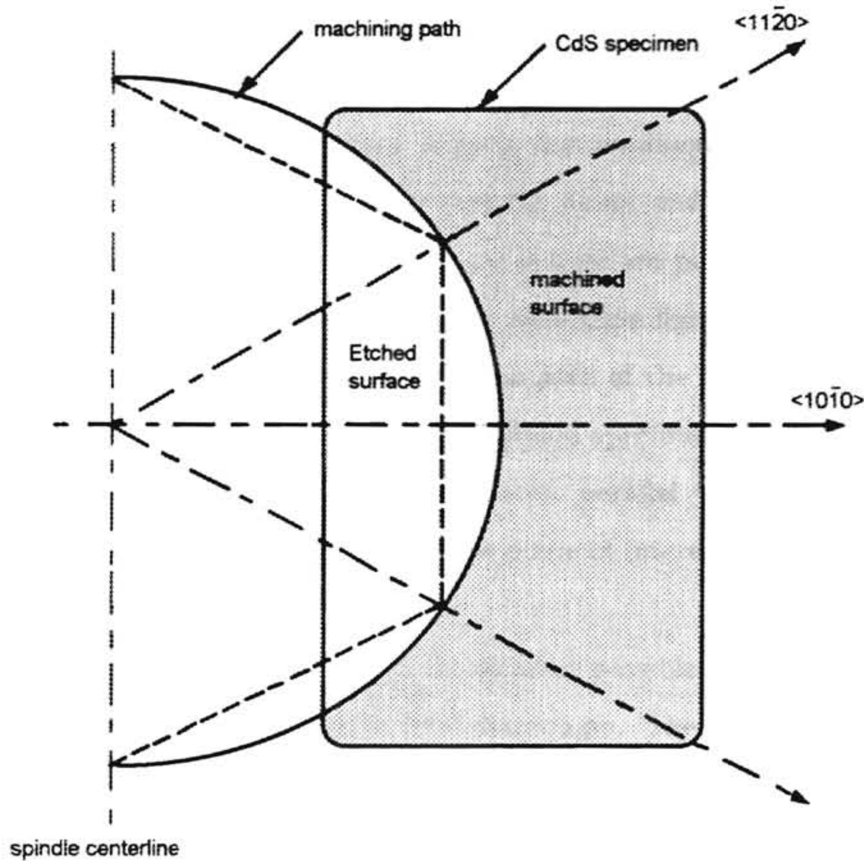

Figure 3-6: The (0001)Cd face showing the orientation of the principal planes, machined surface, and etched surface (Lucca, 1995).

such that a measure of original crystal quality could be made. The (0001)Cd face was machined at nominal depths of cut of 0.1, 0.5, 1.25, and 10 μm. The feedrate

was 6.25 μm/rev, and the cutting speed at the crystal centerline was 0.8 m/sec. No lubricant was used. Multiple passes at the final depth of cut were made to assure that the surface was representative of the depth of cut of interest. Greater than 40 times the nominal depth of cut in thickness was removed. The tool used was a single crystal diamond having a nose radius of 5 mm, a 0 degree rake angle and a 5 degree clearance angle. Lucca et al. (1995) note that the edge profile, as measured with an atomic force microscope technique was found to be a true radius of 50 nm $\pm$ 10 nm.

3.3 Fluorescence Intensity Measurements

Centering and focusing of the mercury lamp is first conducted before any intensity measurement is made. This is to ensure that the direct and reflected images of the arc are coincident, and that the coincident arc images are positioned and focused in the center of the illuminated spot. Maximum excitation light is to be incident onto the excitation filter. Therefore, any filter in the path of the excitation light prior to the excitation filter is removed. Next, the machined specimen is oriented on the x-y table of the microscope with the plane of interest parallel to the y-axis of the x-y table. The schematic of the orientation of the plane of interest parallel to the y-axis is shown in Figure 3-7.

In taking the intensity measurement, the smallest possible illuminated spot on the specimen is obtained by adjusting the field diaphragm. The diameter of the illuminated spot was measured to be about 9.7 μm and is used throughout the experiments. The measurement of the illuminated spot size was obtained by first calibrating the microscope with a standard grating via the calibration tool in the imaging software. The spot diameter was then measured with the measurement tool in the software.

After the specimen has been oriented, the objective is removed and the specimen is exposed to the excitation light for a duration of one hour, two hours, or three hours. After the specimen is exposed for one hour, the objective is replaced and the

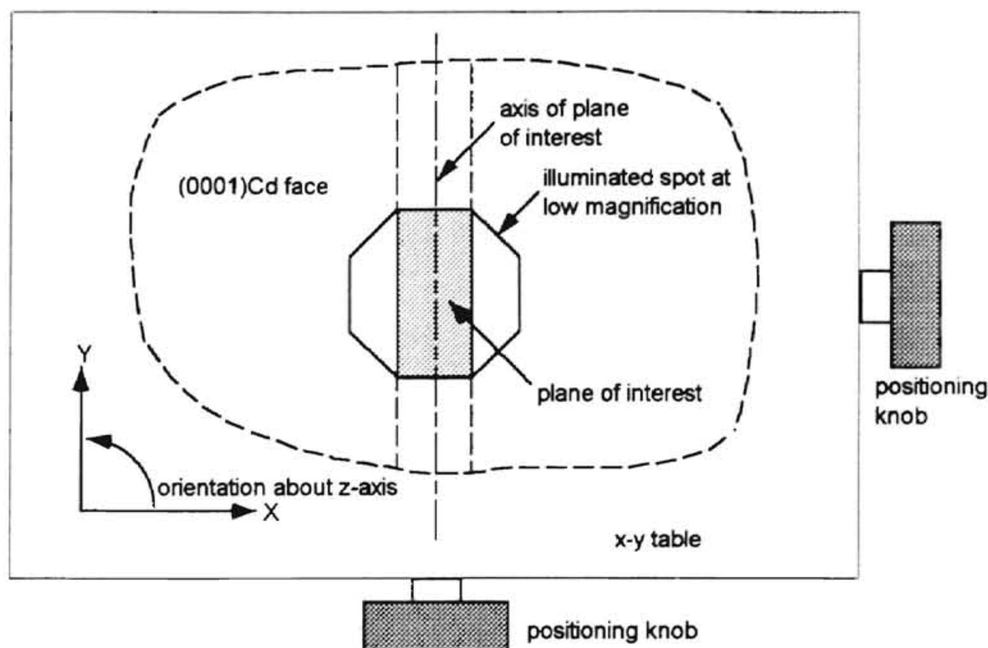

Figure 3-7: Schematic of the orientation of the plane of interest parallel to the y-axis of the microscope x-y table.

illuminated spot is focused at 1000× magnification. The imaging software is then activated to digitize and capture the illuminated spot. The software's histogram tool is then used to measure the mean intensity of the illuminated spot. The distribution of the intensity in the rectangular region of interest, ROI, in terms of grayscale value can be determined using the histogram tool. The rectangular ROI used in the study has a width of 1.4 μm and a height of 5.3 μm, and contains 240 pixels. The distribution of the intensity within the ROI is given both graphically and in terms of statistically analyzed information which includes values of the mean, minimum, maximum, median, and standard deviation of the intensity, and the total number of pixels in the ROI. A display of the histogram feature is shown in Figure 3-8.

The ROI in the illuminated spot is then scanned to a location that gives the lowest standard deviation of the distribution of the gray values. If none is found (i.e., the gray value standard deviation > 3.5) the software is exited, and a new illuminated spot

OKLAHOMA STATE UNIVERSITY

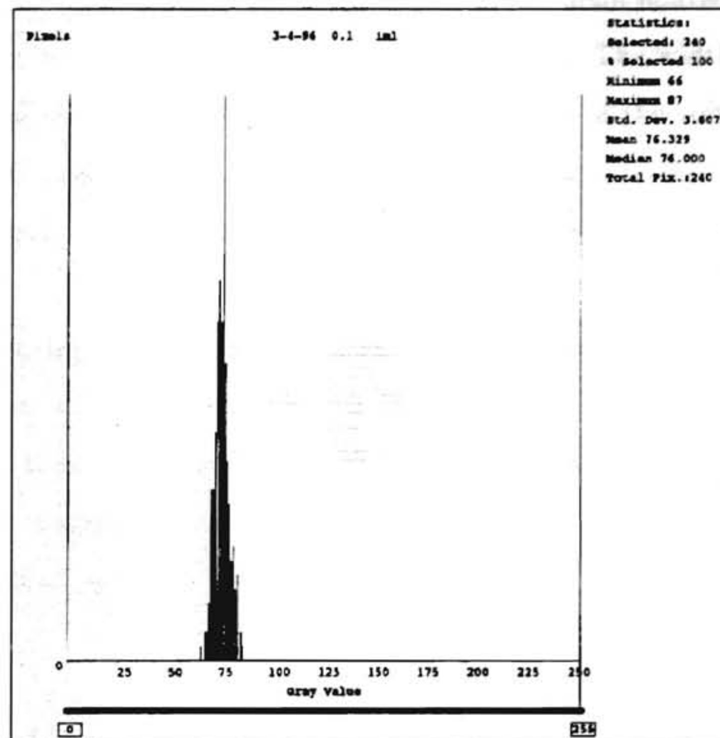

Figure 3-8: A display of the software histogram tool which gives both the graphical and statistically analyzed information.

on the specimen is located by positioning counterclockwise a quarter turn (resulting in a translational displacement of 0.3 mm) via the y-axis positioning knob. The standard deviation of 3.5 gray value represents 5 percent of the mean intensity of the ROI. For one specimen under study, ten intensity readings and their respective standard deviations are recorded. The first five readings are taken at locations which are progressively extended within the machined surface, and the last five readings are taken at locations which are progressively withdrawn toward the machined-etched boundary.

Central to the accuracy and repeatability of the measurements is the minimization of both the illuminated spot and the ROI. The illuminated spot is controlled by the field diaphragm and the smallest achievable diameter is 9.7 μm. The ROI derived from the histogram tool of the imaging software is superimposed on the digitized

illuminated spot. The dimensions of the ROI can be manipulated by the imaging software. The ROI is chosen to have a rectangular shape. The width of the rectangle is made to be as small as possible within the constraints of the software. The longitudinal axis of the rectangular ROI is made to orient in-line to the specimen plane of interest, such that the ROI captures the fluorescence intensity representative of that region.

The spatial extent of the effect of dislocations on fluorescence intensity has been studied by Böhm and Fischer (1979). In their study on PL at dislocations in GaAs they found that the contrast at individual dislocations varies between $C = 0$ and $C = 0.5$ for different samples, as well as for different dislocations in the very same sample. They defined contrast, C, as

$$C = \frac{I_0 - I_D}{I_0} \tag{3.1}$$

where I_0 is the luminescence intensity outside the core of the dislocation and I_D is the luminescence intensity at the core of the dislocation. The researchers have noted that the spatial extent of the contrast, measured by the half width of a dip in luminescence intensity, such as shown in Figure 3-9, ranged from 5-15 μm. In addition, they have observed that the PL spectra at the core and outside the dislocations differed only in overall intensity, but no changes in the relative intensities of the various lines in the spectrum occurred.

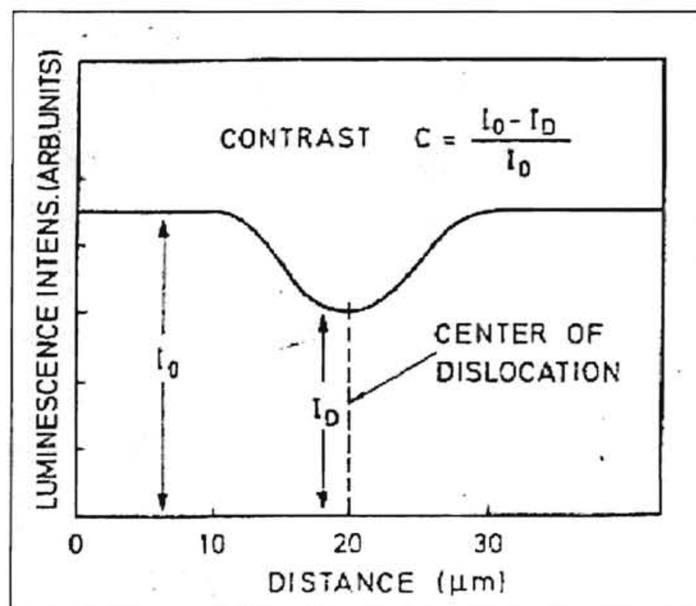

Figure 3-9: Typical luminescence profile (schematic) as a function of distance across a dislocation (Böhm and Fischer, 1979).

Chapter 4

Results and Discussion

In this study, room temperature fluorescence intensity measurements were performed along the $(10\bar{1}0)$ and $(11\bar{2}0)$ planes of CdS specimens that had been machined at 0.1, 0.5, 1.25, and 10 μm depth of cut. Exposure times to ultraviolet light (UV) in the wavelength range of 400-440 nm were one hour, two hours and three hours . In addition, intensity measurements were made on a chemo-mechanically polished CdS specimen of a different bulk CdS crystal of nominal dimensions 20 mm $\times$ 25 mm $\times$ 2 mm. A repeatability study was made for each depth of cut along the $(10\bar{1}0)$ plane. When the specimens were prepared, all machining parameters other than the depth of cut were kept the same. Intensity measurements were taken at ambient conditions in a dark room.

The imaging software evaluates the mean intensity over the ROI. Shown in Figure 4-1 is the measured mean fluorescence intensity obtained from a chemo-mechanically polished CdS specimen measured at different illuminated spot locations at various durations of exposure to UV light. In the figure, the observation depicts the number of instant the mean fluorescence intensity reading is recorded after exposure to each duration. Figure 4-2 shows the mean intensity of the same chemo-mechanically polished CdS specimen, measured at the same illuminated spot location at various durations of exposure to UV light as indicated by data set 1, and at one hour of

exposure to UV light at a different day as indicated by data set 2. Table 4-1 gives the comparison between the measurements in terms of the mean intensity and percent change. From Table 4-1, the difference in percent change in the mean intensity for the specimen measured after 2 hours and after 3 hours at different illuminated spot locations is less than 1 percent whereas that of the specimen measured at same illuminated spot location is 1.9 percent, which is almost double the previous case. Since the percent change is less than 1 percent for the specimen measured at different illuminated spot locations, it is assumed that after 3 hours of exposure to UV light, the mean intensity has stabilized. The mean intensity of the specimen measured at the same illuminated spot location is observed to be higher than that for the specimen measured at different illuminated spot locations for all the durations of exposure. This comparative study indicates that the measurement of mean intensity should be taken after 3 hours of exposure to UV light and that the measurement can be averaged over different illuminated spots.

Figures 4-3 to Figure 4-6 show the mean intensity from $\langle 0001 \rangle$ CdS machined along the $(10\bar{1}0)$ plane at depths of cut of 0.1, 0.5, 1.25, and 10.0 μm respectively at various durations of exposure to UV light. Also included in each figure is the mean intensity measurement after exposure for 3 hours taken on a different day (data set 2). Tables 4-2 to 4-5 give the summary of the mean and standard deviation of the data in Figures 4-3 to 4-6.

Figure 4-7 shows the mean intensity from $\langle 0001 \rangle$ CdS machined along the $(10\bar{1}0)$ plane at depths of cut of 0.1, 0.5, 1.25, and 10.0 μm measured after 3 hours of exposure to UV light. Table 4-6 gives a summary of the mean and standard deviation of the data in Figure 4-7. Figure 4-8 shows the mean intensity from $\langle 0001 \rangle$ CdS machined along the $(11\bar{2}0)$ plane at depths of cut of 0.1, 0.5, 1.25, and 10.0 μm measured after 3 hours of exposure to UV light. Table 4-7 gives a summary of the mean and standard deviation of the data in Figure 4-8. Figure 4-9 shows the average values of mean intensity from $\langle 0001 \rangle$ CdS machined along the $(10\bar{1}0)$ and $(11\bar{2}0)$ planes at depths of

cut of 0.1, 0.5, 1.25, and 10.0 μm measured after 3 hours of exposure to UV light. Table 4-8 gives a summary of the mean intensity data in Figure 4-9.

When one compares the data presented in Figure 4-9 with the results reported by Lucca et al. (1996) as in Figure 4-11, it appears that the mean fluorescence intensity is able to distinguish the degree of lattice disorder in the subsurface of the $\langle 0001 \rangle$ CdS machined along the $(10\bar{1}0)$ and $(11\bar{2}0)$ planes for various depths of cut. The present fluorescence study shows that the degree of lattice disorder in the subsurface is the least at 0.1 μm depth of cut for both the $(10\bar{1}0)$ and $(11\bar{2}0)$ planes. As the depth of cut increases the mean fluorescence intensity reduces, inferring that the degree of lattice disorder has correspondingly increased. The mean intensity then increases beyond the depth of cut of 1.25 μm which indicates that the mean intensity has reached a minimum between a depth of cut of 1.25 and 10.0 μm.

Lucca et al. (1996) in their study of the subsurface damage distribution in ultraprecision machined CdS have made a comparison of the damage depth profiles for a range of depths of cut for machining along the $(10\bar{1}0)$. They have shown that at a particular depth from the surface, the relative disorder of the lattice increases with depth of cut up to a depth of about 320 nm as shown in Figure 4-10. In the same study, the group observed, using ion channeling, that there is a larger depth of damage for the CdS machined along the $(10\bar{1}0)$ plane as compared to the $(11\bar{2}0)$ plane. The general trend of increased damage with depth of cut up to 1.25 μm can be seen from Figure 4-11. It is less clear whether their measurements are consistent with the fluorescence results at 10.0 μm, however, the ion channeling results show that a reduction in damage depth at 10.0 μm depth of cut is plausible.

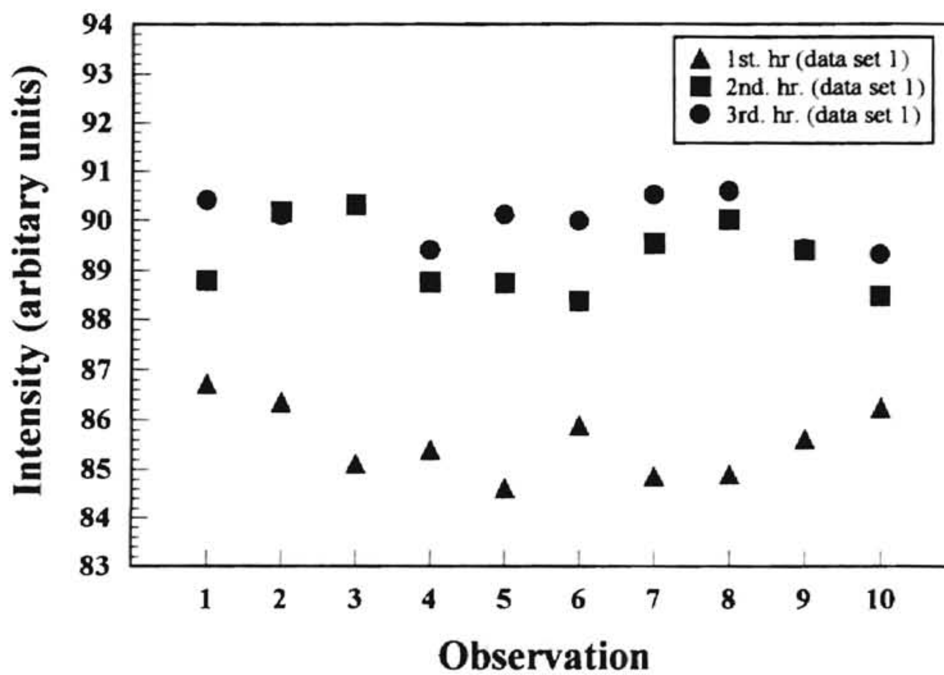

Figure 4-1: Mean fluorescence intensity from a chemo-mechanically polished CdS specimen measured at various locations and durations of exposure to UV light.

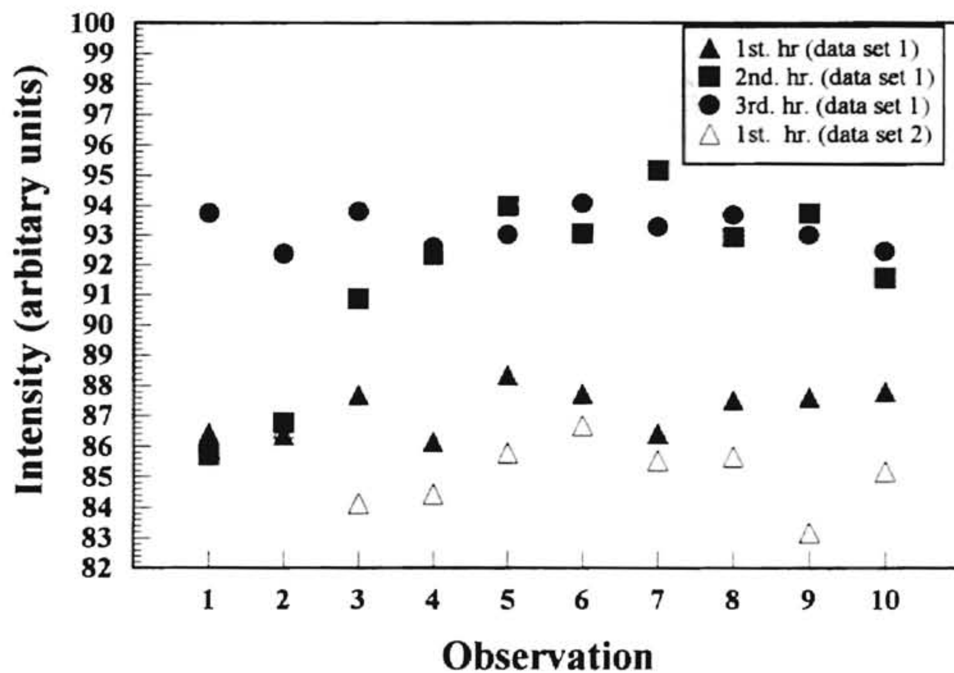

Figure 4-2: Mean fluorescence intensity from a chemo-mechanically polished CdS specimen (same as specimen of Figure 4-1) measured at same location and various durations of exposure to UV light.

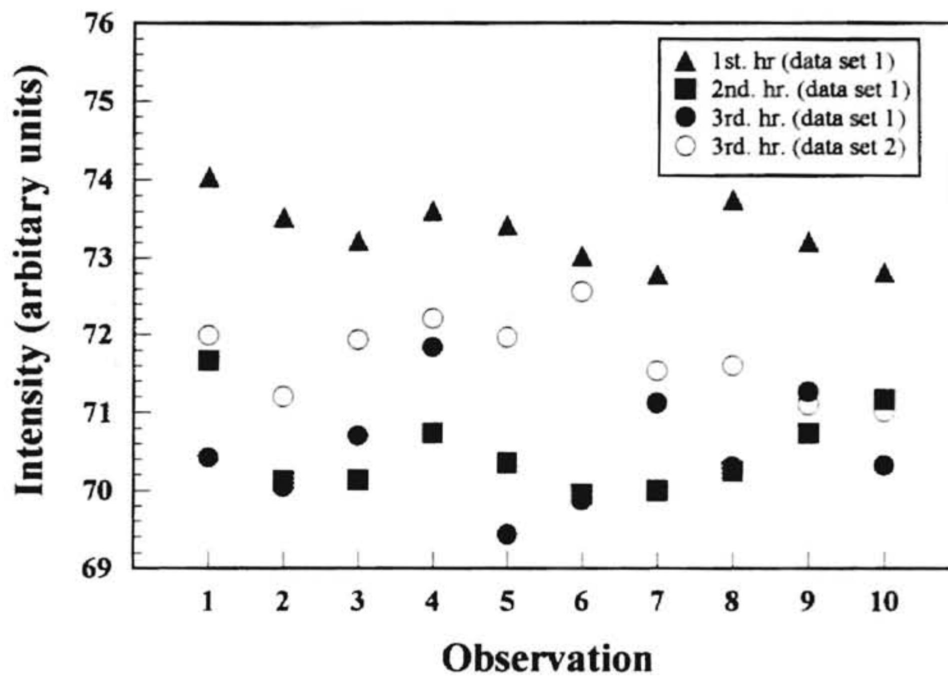

Figure 4-3: Mean fluorescence intensity from ⟨0001⟩ CdS machined along ⟨10$\bar{1}$0⟩ at a depth of cut of 0.1 μm at various durations of exposure to UV light.

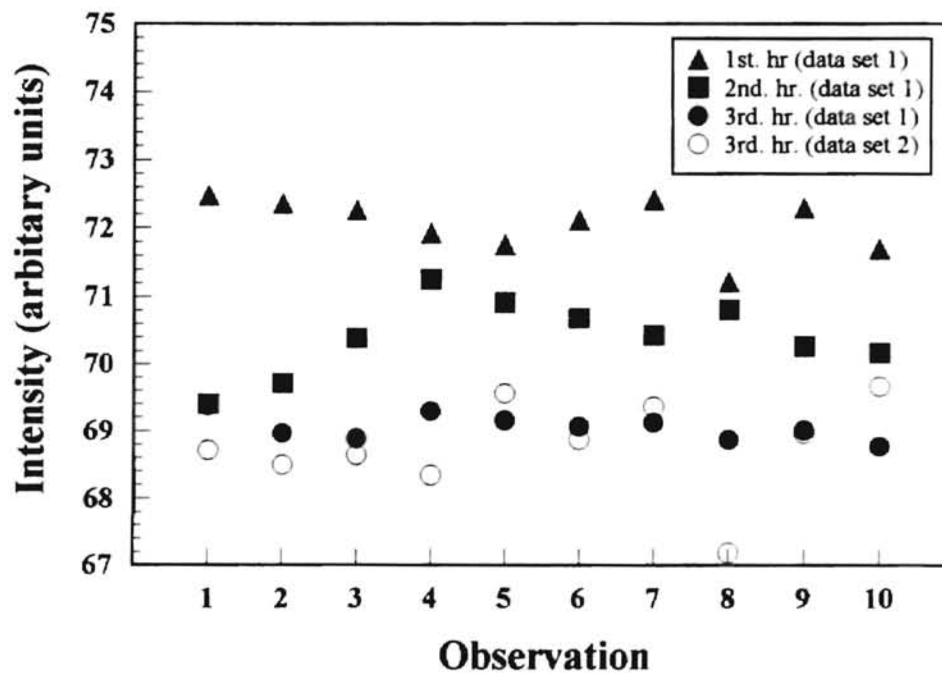

Figure 4-4: Mean fluorescence intensity from ⟨0001⟩ CdS machined along $(10\bar{1}0)$ at a depth of cut of 0.5 μm at various durations of exposure to UV light.

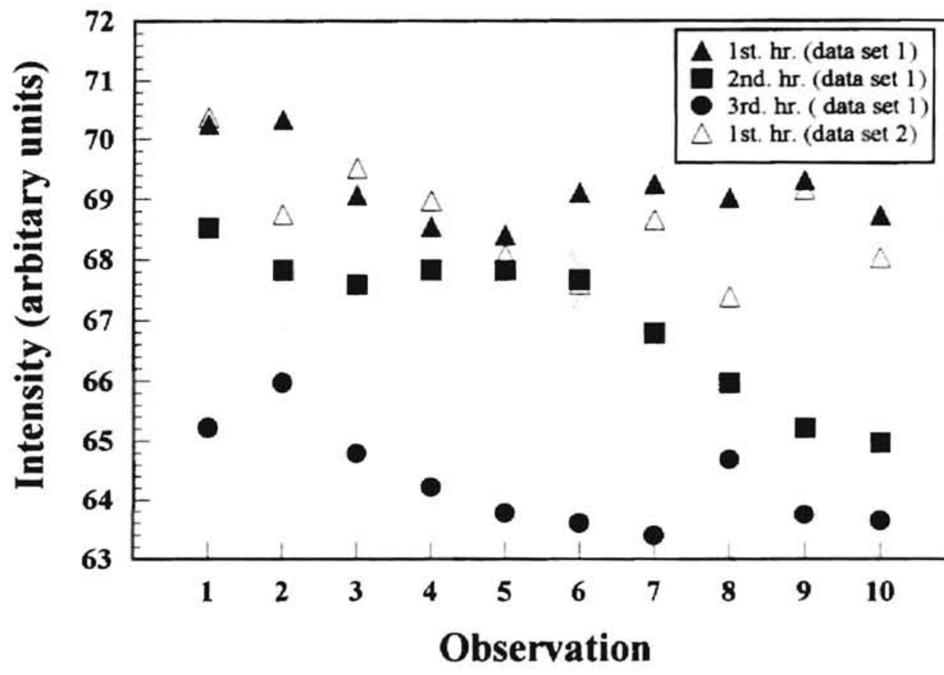

Figure 4-5: Mean fluorescence intensity from $\langle 0001 \rangle$ CdS machined along $(10\bar{1}0)$ at a depth of cut of 1.25 μm at various durations of exposure to UV light.

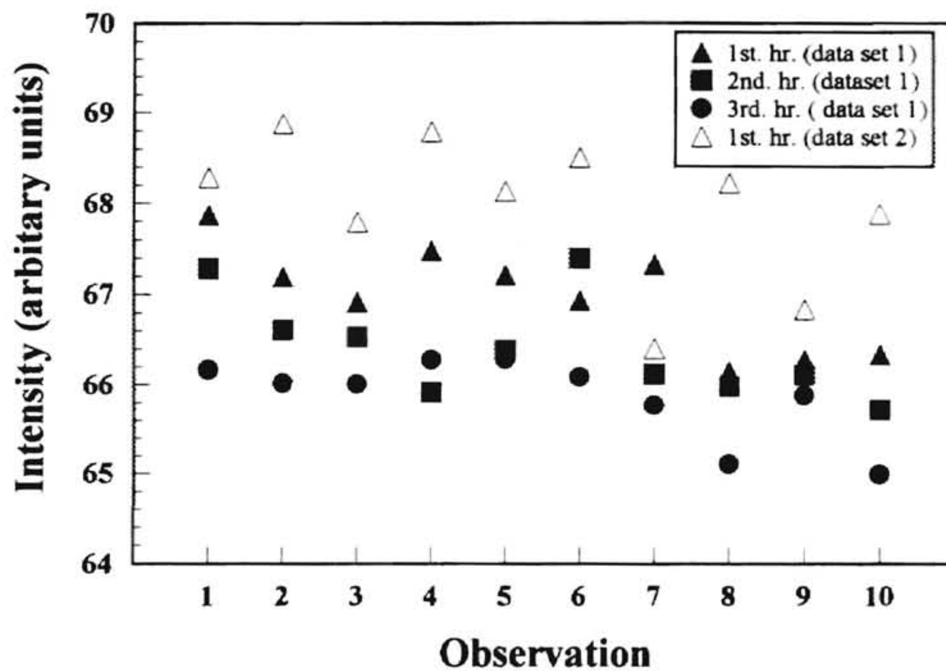

Figure 4-6: Mean fluorescence intensity from ⟨0001⟩ CdS machined along ⟨$10\bar{1}0$⟩ at a depth of cut of 10.0 μm at various durations of exposure to UV light.

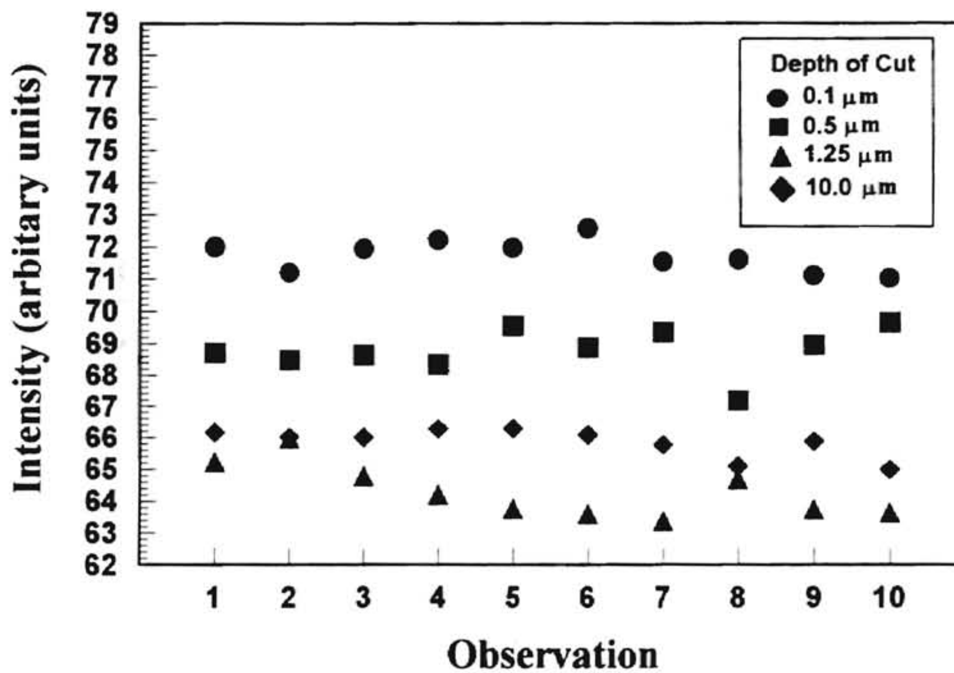

Figure 4-7: Mean fluorescence intensity from ⟨0001⟩ CdS machined along $(10\bar{1}0)$ at various depths of cut measured after 3 hours of exposure to UV light.

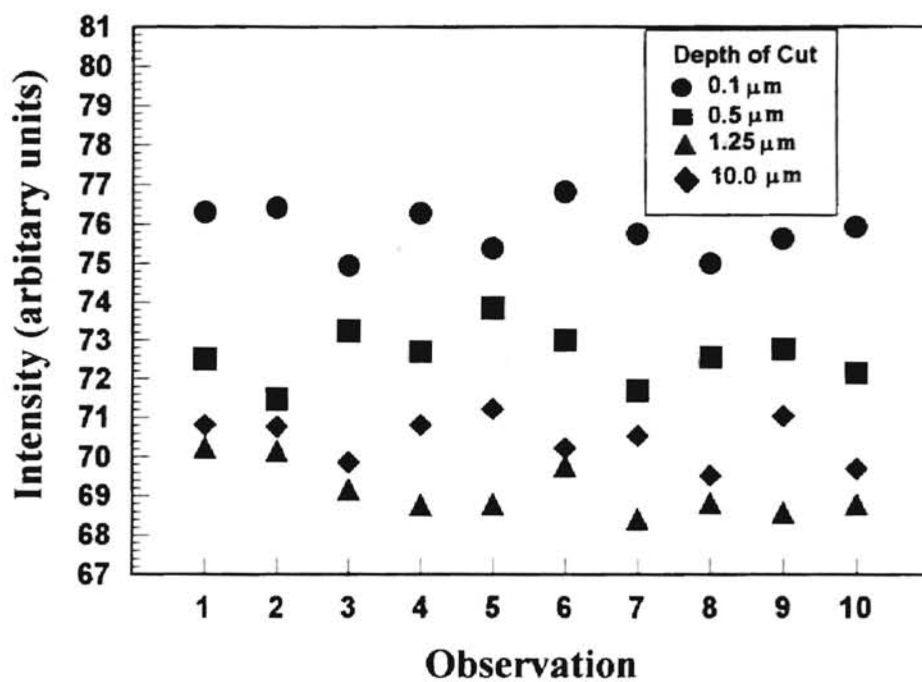

Figure 4-8: Mean fluorescence intensity from ⟨0001⟩ CdS machined along $(11\bar{2}0)$ at various depths of cut measured after 3 hours of exposure to UV light.

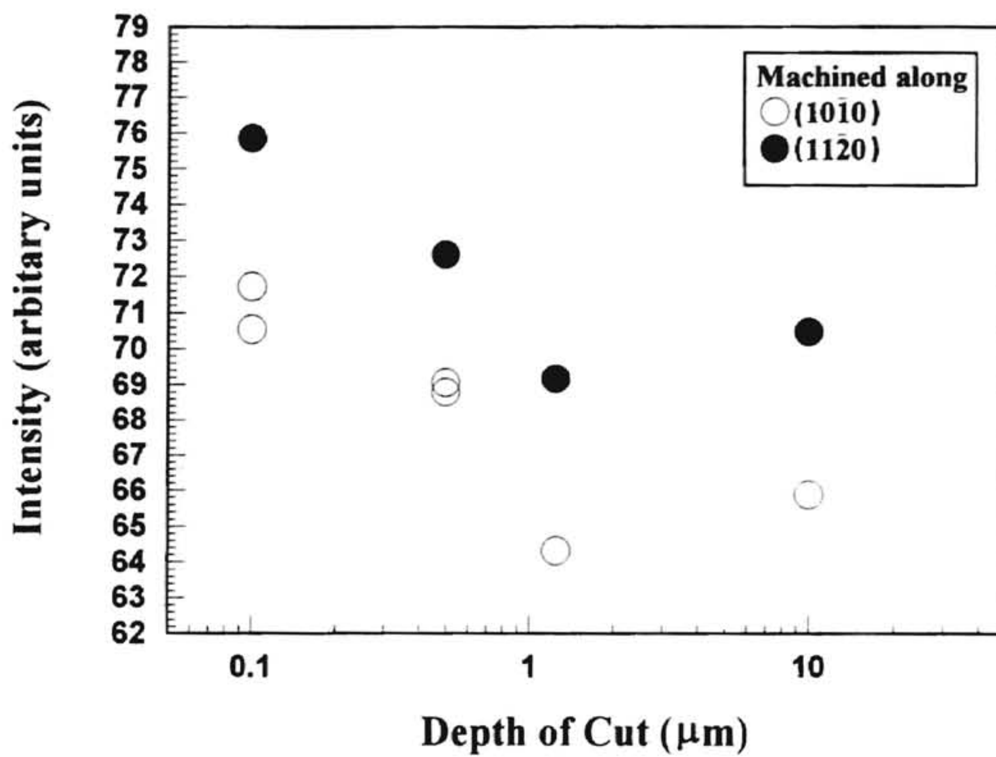

Figure 4-9: Mean fluorescence intensity from ⟨0001⟩ CdS machined along (10$\bar{1}$0) and (11$\bar{2}$0) at various depths of cut measured after 3 hours of exposure to UV light.

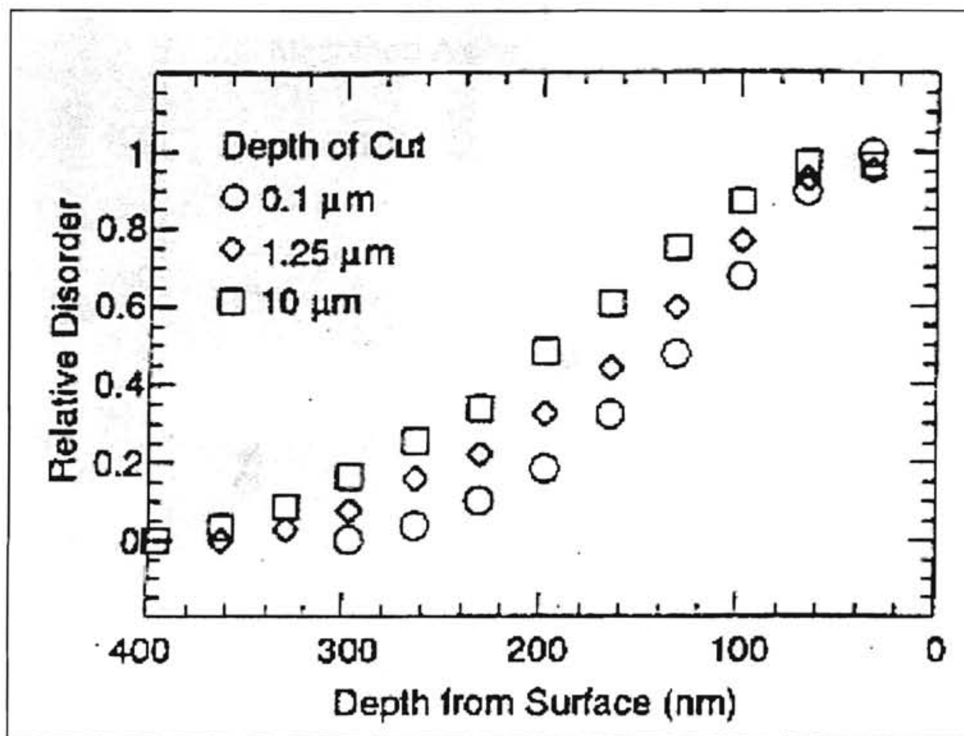

Figure 4-10: Comparison of depth profiles for ⟨0001⟩ aligned CdS diamond turned along a preferred cleavage plane, $(10\bar{1}0)$, at various depths of cut. (Lucca et al, 1996)

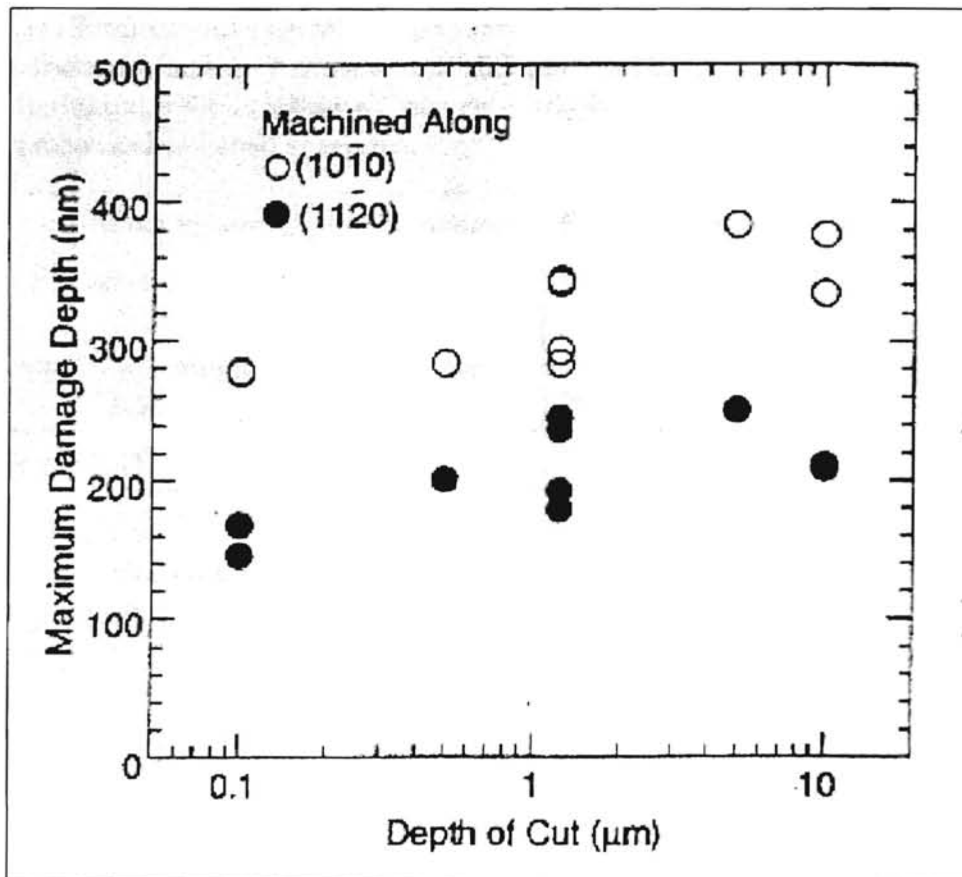

Figure 4-11: Maximum damage depth for ⟨0001⟩ CdS machined along the (10$\bar{1}$0) and (11$\bar{2}$0) planes at various depths of cut. (Lucca et al., 1996)

Illuminated spot location	Mean intensity (1 hr.) (A)	Mean intensity (2 hrs.) (B)	% change ($\frac{B-A}{A}$ ×100%)	Mean intensity (3 hrs.) (C)	% change ($\frac{C-A}{A}$ ×100%)
Different location	85.6	89.2	4.2	90.0	5.1
Same location	87.2	91.6	5.0	93.2	6.9

Table 4.1: Summary of the mean, standard deviation, and percent change of the mean fluorescence intensity measured at different illuminated spot locations and the same illuminated spot location at various durations of UV light exposure for the chemo-mechanical polished specimen.

	Mean intensity after 1 hr.	Mean intensity after 2 hrs.	Mean intensity after 3 hrs.	Mean intensity after 3 hrs. (on different day)
	73.34	70.51	70.53	71.71
Std. dev.	0.41	0.56	0.72	0.51

Table 4.2: Summary of the mean and standard deviation of the fluorescence intensity measured at various durations of UV light exposure from $\langle 0001 \rangle$ CdS machined along $(10\bar{1}0)$ at a depth of cut of 0.1 μm.

	Mean intensity after 1 hr.	Mean intensity after 2 hrs.	Mean intensity after 3 hrs.	Mean intensity after 3 hrs. (on different day)
	72.05	70.40	69.04	68.77
Std. dev.	0.40	0.56	0.19	0.71

Table 4.3: Summary of the mean and standard deviation of the fluorescence intensity measured at various durations of UV light exposure from $\langle 0001 \rangle$ CdS machined along $(10\bar{1}0)$ at a depth of cut of 0.5 μm.

	Mean intensity after 1 hr.	Mean intensity after 2 hrs.	Mean intensity after 3 hrs.	Mean intensity after 1 hr. (on different day)
	69.21	67.02	64.31	68.65
Std. dev.	0.65	1.23	0.84	0.92

Table 4.4: Summary of the mean and standard deviation of the fluorescence intensity measured at various durations of UV light exposure from $\langle 0001 \rangle$ CdS machined along $(10\bar{1}0)$ at a depth of cut of 1.25 μm.

	Mean intensity after 1 hr.	Mean intensity after 2 hrs.	Mean intensity after 3 hrs.	Mean intensity after 1 hr. (on different day)
	66.97	66.40	65.86	67.97
Std. dev.	0.56	0.57	0.46	0.80

Table 4.5: Summary of the mean and standard deviation of the fluorescence intensity measured at various durations of UV light exposure from $\langle 0001 \rangle$ CdS machined along $(10\bar{1}0)$ at a depth of cut of 10.0 μm.

	Mean intensity			
Depth of cut, μm	0.1	0.5	1.25	10.0
	71.71	68.77	64.31	65.86
Std. dev.	0.51	0.71	0.84	0.46

Table 4.6: Summary of the mean and standard deviation of the fluorescence intensity from $\langle 0001 \rangle$ CdS machined along $(10\bar{1}0)$ measured at various depths of cut exposed to 3 hours of UV light.

	Mean intensity			
Depth of cut, μm	0.1	0.5	1.25	10.0
	75.84	72.60	69.16	70.45
Std. dev.	0.62	0.70	0.66	0.59

Table 4.7: Summary of the mean and standard deviation of the fluorescence intensity from $\langle 0001 \rangle$ CdS machined along $(11\bar{2}0)$ measured at various depths of cut exposed to 3 hours of UV light.

Depth of cut, μm	Mean intensity,		
	machined along $(10\bar{1}0)$	machined along $(11\bar{2}0)$	machined along $(10\bar{1}0)$ (on different day)
0.1	71.71	75.84	70.53
0.5	68.77	72.60	69.04
1.25	64.31	69.16	
10.0	65.86	70.45	

Table 4.8: Summary of the mean fluorescence intensity from $\langle 0001 \rangle$ CdS machined along $(10\bar{1}0)$ and $(11\bar{2}0)$ measured at various depths of cut exposed to 3 hours of UV light.

Chapter 5

Conclusion

From the present experiments, it was observed that the chemo-mechanically polished CdS specimen results in a higher mean fluorescence intensity than those CdS crystals which have been diamond turned. Comparing the various depths of cut ranging from 0.1 μm to 10.0 μm in the SPDT of single crystal (0001)-oriented CdS, it was observed that the depth of cut of 0.1 μm gives the highest mean fluorescence intensity and this intensity decreases as the depth of cut increases to 1.25 μm. Beyond this the mean fluorescence intensity increases as the depth of cut increases to 10.0 μm. Comparing the CdS crystals machined along the $(10\bar{1}0)$ and $(11\bar{2}0)$ planes for depths of cut ranging from 0.1 μm to 10.0 μm, it was observed that the crystals machined along the $(11\bar{2}0)$ plane consistently gave higher PL intensities than those machined along the $(10\bar{1}0)$ plane.

The first observation indicates that chemo-mechanical polishing produces less subsurface damage than the SPDT process. The second observation indicates that subsurface damage increases as the depth of cut increases up to a depth of cut of about 1.25 μm. The third observation indicates that single point diamond turning along the $(10\bar{1}0)$ plane produces more subsurface damage than when machining along the $(11\bar{2}0)$ plane. The results of the present study are consistent with studies of the depth of subsurface damage of the same crystals performed by ion channeling (Lucca

et al., 1995, 1996). A review of the literature has indicated that there are a number of possible mechanisms for luminescence quenching around dislocations, and it is not certain which is the exact mechanism that gives rise to the above observations. Finally the present experiments have indicated that fluorescence microscopy at ambient conditions can be used to evaluate the subsurface damage of single crystal CdS.

The measurement of the fluorescent intensity in this thesis encompasses the broad spectrum of wavelengths in excess of 470 nm. Future work should then concentrate on measuring fluorescent intensity at a narrow band of the fluorescent spectrum. In addition, measurement of fluorescent intensity at the "dislocation emission", which has been identified by Negrii (1992) to be a characteristic group of emission lines in the 505 nm and 515 nm region of the low temperature PL spectrum of CdS, should be explored.

Bibliography

[1] Fluorescence microscopes. Technical report, Nikon Corporation, 1991.

[2] H. B. Bebb and E. W. Williams. Photoluminescence I: Theory. In R. K. Willardson and A. C. Beer, editors, *Semiconductors and Semimetals*, volume 8, pages 181–320. Academic Press, New York, 1972.

[3] W. S. Blackley and R. O. Scattergood. Crystal orientation dependence of machining damage - a stress model. *Journal of the American Ceramic Society*, 73(10):3113–3115, 1990.

[4] G. Blasse and B. C. Grabmaier. *Luminescent Materials*. Springer-Verlag, New York, 1994.

[5] C. E. Bleil and J. W. A. Albers. The influence of ambient atmospheres on the exciton emission of cadmium sulfide. *Surface Science*, 2:307–313, 1964.

[6] K. Bohm and B. Fischer. Photoluminescence at dislocations in GaAs and InP. *Journal of Applied Physics*, 50(8):5453–5460, 1979.

[7] M. Bujatti. Surface effects and the absorption edge of CdS. *Journal of Applied Physics*, 40(7):2965–2967, 1969.

[8] P. J. Dean, D. C. Herbert, C. J. Werkhoven, B. J. Fitzpatrick, and R. N. Bhargava. Donor bound-exciton excited states in zinc selenide. *Physical Review B*, 23(10):4888–4901, 1981.

[9] I. B. Ermolovich, G. P. Peka, and M. K. Sheinkman. Effect of surface states on luminescent properties of CdS single crystals. *Surface Science*, 24:229–238, 1971.

[10] T. J. Garosshen, C. S. Kim, and J. M. Galligan. On the influence of light on dislocation motion in compound semiconductors. *Journal of Electronics Materials*, 19(9):889–894, 1990.

[11] D. Guidotti, E. Hassan, H. J. Hovel, and M. Albert. Degradation of band-gap photoluminescence in GaAs. *Applied Physics Letters*, 50(14):912–914, 1987.

[12] D. Guidotti and H. J. Hovel. Model for degradation of band-gap photoluminescence in GaAs. *Applied Physics Letters*, 53(15):1411–1413, 1988.

[13] R. E. Halsted. Radiative recombination in the band edge region. In M. Aven and J. S. Prener, editors, *Physics and Chemistry of II-VI Compounds*, pages 385–429. John Wiley and Sons, New York, 1967.

[14] G. Heine and K. Wandel. The influence of chemisorption of oxygen on the luminescence of CdS single crystals. *Physica Status Solidi (A)*, 19:415–421, 1973.

[15] C. H. Henry, K. Nassau, and J. W. Shiever. Double-donor-acceptor pair lines and the chemical identification of the I1 lines in CdS. *Physical Review Letters*, 24(15):820–822, 1970.

[16] J. J. Hopfield. The quantum chemistry of bound exciton complexes. *Proceedings of the International Conference on Physics of Semiconductors, Paris*, pages 725–735, 1964.

[17] H. J. Hovel. Scanned photoluminescence of semiconductors. *Semiconductor Science and Technology*, 7:A1–A9, 1992.

[18] G. F. Imbusch. Inorganic luminescence. In M. D. Lump, editor, *Luminescence Spectroscopy*, pages 1–92. Academic Press, London, 1978.

[19] S. Y. Kim, D. S. Kim, B. T. Ahn, and H. B. Im. Electrical and optical properties of vacuum-evaporated cds films. *Journal of Materials Science: Materials in Electronics*, 4:178–182, 1993.

[20] G. Leo, A. V. Drigo, N. Lovergine, and A. M. Mancini. Structural characteristic of CdS epilayers by channeling rutherford backscattering spectrometry. *Journal of Applied Physics*, 70(4):2041–2045, 1991.

[21] S. H. Liebson. Surface states of cadmium sulfide. *Journal of the Electrochemical Society*, 101(7):359–362, 1954.

[22] S. H. Liebson. Surface recombination of cadmium sulfide. *Journal of Chemical Physics*, 23:1732, 1955.

[23] S. H. Liebson and E. J. West. Effect of oxygen on luminescence of cadmium sulfide. *Journal of Chemical Physics*, 23:977–978, 1955.

[24] D. A. Lucca. *(unpublished work)*, 1995.

[25] D. A. Lucca, C. J. Maggiore, and R. L. Rhorer. Subsurface damage distribution in ultraprecision machined CdS. *Annals of the CIRP*, 45(1):519–522, 1996.

[26] D. A. Lucca, R. L. Rhorer, C. J. Maggiore, and Y. W. Seo. Assessment of subsurface damage in ultraprecision-machined CdS by ion channeling. *Annals of the CIRP*, 44(1):513–516, 1995.

[27] H. Luo and J. K. Furdyna. The II-VI semiconductor blue-green laser: Challenges and solutions. *Semiconductor Science and Technology*, 10:1041–1048, 1995.

[28] A. Many and A. Katzir. Surface states on the (0001) faces of cadmium crystal. *Surface Science*, 6:279–292, 1967.

[29] H. Mar. Optical properties of the wide bandgap II-VI semiconductors. In H. E. Ruda, editor, *Widegap II-VI Compounds for Opto-electronic Application*, pages 167–188. Chapman Hall, London, 1992.

[30] J. C. Morris and D. L. Callahan. Origins of microplasticity in low-load scratching of silicon. *Journal of Materials Research*, 9(11):2907–2913, 1994.

[31] J. C. Morris, D. L. Callahan, J. Kulik, J. A. Patten, and R. O. Scattergood. Origins of ductile regime in single-point diamond turning of semiconductors. *Journal of the American Ceramic Society*, 78(8):2015–2020, 1995.

[32] V. D. Negrii. Dynamic and optical properties of screw dislocations introduced by plastic deformation of cds crystals at 77-4.2 k. *Journal of Crystal Growth*, 117:672–676, 1992.

[33] O. Parillaud, E. Gil-Lafon, B. Gerard, and D. Pribat. High quality InP on Si by conformal growth. *Applied Physics Letter*, 68 (19):2654–2656, 1996.

[34] S. Perkowitz, D. G. Seiler, and W. M. Duncan. Optical characterization in microelectronics manufacturing. *Journal of Research of the National Institute of Standards and Technology*, 99(5):605–639, 1994.

[35] J. S. Ploem and H. J. Tanke. *Introduction to Fluorescence Microscopy*. Oxford University Press, Oxford, 1987.

[36] D. Pribat, B. Gerard, M. Dupuy, and P. Legagneux. High quality GaAs on Si by conformal growth. *Applied Physics Letter*, 60 (17):2144–2146, 1992.

[37] K. E. Puttick and M. M. Hosseini. Fracture by a pointed indenter on near (111) silicon. *Journal of Physics D: Applied Physics*, 13:875–880, 1980.

[38] K. E. Puttick, L. C. Whitmore, C. L. Chao, and A. E. Gee. Transmission electron microscopy of nanomachined silicon crystals. *Philosophical Magazine A*, 69(1):91–103, 1994.

[39] K. E. Puttick, L. C. Whitmore, P. Zhdan, A. E. Gee, and C. L. Chao. Energy scaling transitions in machining of silicon by diamond. *Tribology International*, 28(6):349–355, 1995.

[40] F. W. D. Rost. *Fluorescence Microscopy*, volume 1. Cambridge University Press, Cambridge, 1992.

[41] C. G. Scott and C. E. Reed. II-VI and III-V compounds materials. In C. G. Scott and R. C. E., editors, *Surface Physics of Phosphors and Semiconductors*, pages 411–521. Academic Press, London, 1975.

[42] Y. G. Shreter, Y. T. Rebane, O. V. Klyavin, P. S. Aplin, C. J. Axon, W. T. Young, and J. W. Steeds. Dislocation-related absorption and photoluminescence in deformed n-ZnSe crystals. *Journal of Crystal Growth*, 159:883–888, 1996.

[43] K. J. Stine and C. M. Knobler. Fluorescence microscopy: A tool for studying the physical chemistry of interfaces. *Ultramicroscopy*, 47:23–34, 1992.

[44] T. Suzuki and M. Ogawa. Degradation of photoluminescence intensity caused by excitation-enhanced oxidation of GaAs surfaces. *Applied Physics Letters*, 31(7):473–475, 1977.

[45] K. Vaccaro, A. Davis, H. M. Dauplaise, S. M. Spaziani, E. A. Martin, and J. P. Lorenzo. Cadmium sulfide surface stabilization for InP-based optoelectronic devices. *Journal of Electronic Materials*, 25(4):603–609, 1996.

[46] G. A. Wolff and J. D. Broder. Microcleavage, bonding character and surface structure in materials with tetrahedral coordination. *Acta Crystallography*, 12:313–323, 1959.

2

Vita

Kim-Cheng Tan

Candidate for the Degree of

Master of Science

Thesis: ASSESSMENT OF SUBSURFACE DAMAGE IN ULTRAPRECISION MACHINED CADMIUM SULFIDE BY FLUORESCENCE MICROSCOPY

Major Field: Mechanical Engineering

Biography:

Education: Received Bachelor of Science in Mechanical Engineering from Oklahoma State University, Stillwater, Oklahoma in May 1986. Completed the requirements for the Master of Science degree with a major in Mechanical Engineering at Oklahoma State University in October 1996.

Experience: Research assistant, Oklahoma State University, Stillwater, Oklahoma, June 1996 to August 1996; teaching assistant, Oklahoma State University, Stillwater, Oklahoma, August 1995 to May 1996; lecturer, Temasek Polytechnic, Singapore, March 1992 to December 1994; senior engineer, Printronix AG, Singapore, October 1989 to February 1992; development engineer II, Digital Equipment International Limited, Singapore, April 1987 to September 1989; teaching assistant, Oklahoma State University, Stillwater, Oklahoma, August 1986 to December 1986; apprentice aircraft maintenance engineer, Singapore Airlines Limited, Singapore, June 1979 to June 1982; platoon commander and administration officer, conscripted in the Singapore Armed Forces, December 1976 to June 1979.

Professional Membership: American Society of Mechanical Engineers, Pi Tau Sigma Mechanical Engineering Honors Fraternity.